Available online at www.sciencedirect.com
ScienceDirect
Comput. Methods Appl. Mech. Engrg. 279 (2014) 301–324
Computer methods in applied mechanics and engineering
www.elsevier.com/locate/cma

Model-reduction techniques for Bayesian finite element model updating using dynamic response data

H.A. Jensen[a,*], E. Millas[a], D. Kusanovic[a], C. Papadimitriou[b]

[a] *Department of Civil Engineering, Santa Maria University, Valparaiso, Chile*
[b] *Department of Mechanical Engineering, University of Thessaly, GR-38334 Volos, Greece*

Received 30 January 2014; received in revised form 27 May 2014; accepted 23 June 2014
Available online 26 June 2014

Abstract

This work presents a strategy for integrating a class of model reduction techniques into a finite element model updating formulation. In particular a Bayesian model updating approach based on a stochastic simulation method is considered in the present formulation. Stochastic simulation techniques require a large number of finite element model re-analyses to be performed over the space of model parameters during the updating process. Substructure coupling techniques for dynamic analysis are proposed to reduce the computational cost involved in the dynamic re-analyses. The effectiveness of the proposed strategy is demonstrated with identification and model updating applications for finite element building models using simulated seismic response data.

Keywords: Bayesian updating; Dynamic response; Finite elements; Model reduction techniques; Stochastic simulation

1. Introduction

Model updating using measured system response has a wide range of applications in areas such as structural response prediction, structural control, structural health monitoring, and reliability and risk assessment. [1–7]. For a proper assessment of the updated model all uncertainties involved in the problem should be considered. In fact, there always exist modeling errors and uncertainties associated with the process of constructing a mathematical model of the structure and its future excitation. Thus, the ability to quantify the uncertainties accurately and appropriately is essential for a robust prediction of future responses and reliability of structures [8,9]. In this context a fully probabilistic Bayesian model updating approach provides a robust and rigorous framework for model updating due to its ability to characterize modeling uncertainties associated with the underlying structural system [10,11]. Bayesian probabilistic tools for identifying uncertainty models as well as performing robust prediction analysis are usually based on asymptotic approximations [9,12–14] or stochastic simulation algorithms [15–20]. Asymptotic approximation methods in the Bayesian framework involve solving an optimization problem for finding the most probable model,

* Corresponding author. Tel.: +56 32 2654383; fax: +56 32 2654115.
E-mail address: hector.jensen@usm.cl (H.A. Jensen).

http://dx.doi.org/10.1016/j.cma.2014.06.032
0045-7825/

as well as estimating the Hessian of the logarithm of the posterior probability density function. On the other hand stochastic simulation algorithms involve generating samples for tracing and then populating the important uncertainty region in the parameter space. The application of asymptotic approximation methods faces several difficulties when the chosen class of models is unidentifiable based on the available data [9,21]. Since stochastic simulation algorithms are more general than asymptotic approximation approaches a stochastic simulation algorithm is considered in the present study. In particular the transitional Markov chain Monte Carlo method is implemented here because of its generality and versatility [17]. Such algorithm requires in general a large number of re-analysis to be performed over the space of model parameters. Thus, the computational demands depend on the number of re-analysis and the time required for performing each re-analysis. It is noted that alternative Bayesian model updating techniques can also be used for the identification process. For example the Hybrid Monte Carlo method, which is quite efficient for solving high-dimensional Bayesian model updating problems [17], or the population-based Markov chain Monte Carlo method [20] are certainly alternative choices. The implementation and comparison of different identification tools in the context of model reduction techniques will be the focus of a future work.

The present work proposes to use an efficient model reduction technique to alleviate the computational burden involved in the implementation of the transitional Markov chain Monte Carlo method in the framework of finite element model updating using dynamic response data. Specifically, a class of model reduction techniques known as substructure coupling for dynamic analysis is considered in the present implementation [22]. Such technique can be used to carry out system analysis in a significantly reduced space of generalized coordinates. The methodology is quite useful to efficiently handle the computational effort in system re-analyses that arise from finite element model variations caused by perturbations in the value of the uncertain parameters [23]. Such variations require that the assembly process of the finite element model be repeated in each re-analysis. Clearly, the objective of methods involving dynamic re-analyses of finite element models with varying properties is to control the number of re-analysis of the system.

In this regard, the main objective of this work is to present a strategy for integrating a class of model reduction techniques into a finite element model updating formulation in order to reduce the computational cost involved in the dynamic re-analyses of large scale linear models, including localized nonlinearities. The model reduction technique involves dividing the structural system into a number of linear and nonlinear substructures obtaining reduced-order models of the linear substructures, and then assembling a reduced-order model for the entire structure. It is demonstrated that substantial computational savings are achieved under certain parametrization schemes arising often in finite element model updating formulations.

The organization of this contribution is as follows. Essential aspects of Bayesian finite element model updating using dynamic data are presented in Sections 2 and 3. The mathematical background of the substructure coupling technique for dynamic analysis is outlined in Section 4. The integration of the model reduction technique with the Bayesian model updating approach is discussed in Section 5. The effectiveness of the proposed scheme, in terms of computational efficiency and accuracy is demonstrated in Section 6 with damage identification and model updating applications for finite element building models using simulated seismic response data. The contribution closes with some conclusions and final remarks.

2. Finite element model updating using dynamic response data

2.1. Bayesian formulation

Consider a finite element model class M of a structural system parameterized by a set of model parameters $\boldsymbol{\theta} \in \Theta \subset R^{n_p}$. The plausibility of each model within a class M based on data D is quantified by the updated joint probability density function $p(\boldsymbol{\theta}|M, D)$ (posterior probability density function). By Bayes' Theorem the posterior probability density function of $\boldsymbol{\theta}$ is given by

$$p(\boldsymbol{\theta}|M, D) = \frac{p(D|M, \boldsymbol{\theta})\ p(\boldsymbol{\theta}|M)}{p(D|M)} \tag{1}$$

where $p(D|M)$ is the normalizing constant which makes the probability volume under the posterior probability density function equal to unity, $p(D|M, \boldsymbol{\theta})$ is the likelihood function based on the predictive probability density function for the response given by model class M, and $p(\boldsymbol{\theta}|M)$ is the prior probability density function selected for

the model class M which is used to quantify the initial plausibility of each predictive model defined by the value of the parameters $\boldsymbol{\theta}$, allowing in this manner prior information to be incorporated. In what follows it is assumed that D contains input dynamic data and output responses from measurements on the system. Specifically, let $u_n(t_j, \boldsymbol{\theta})$ denote the output at time t_j at the nth observed degree of freedom predicted by the proposed structural model, and $u_n^*(t_j)$ denote the corresponding measured output. The prediction and measurement errors $e_n(t_j, \boldsymbol{\theta}) = u_n^*(t_j) - u_n(t_j, \boldsymbol{\theta})$ for $n = 1, \ldots, N_o$, and $j = 1, \ldots, N_T$, where N_o denotes the number of observed degrees of freedom and N_T denotes the length of the discrete time history data, are modeled as independent and identically distributed Gaussian variables with zero mean [9,24,25]. This assumption implies stochastic independence of the prediction errors for different channels of measurements and for different time instances. This formulation is based on the maximum entropy principle which yields a multi-dimensional Gaussian distribution for the prediction errors [13,26]. In this context it is noted that different prediction error model classes can be used as well [27]. Using the above probability model for the prediction error it can be shown that the likelihood function $p(D|M, \boldsymbol{\theta})$ can be expressed in terms of a measure-of-fit function $J(\boldsymbol{\theta}|M, D)$ between the measured response and the model response at the measured degrees of freedom. Such function is given by [9,13,14,25]

$$J(\boldsymbol{\theta}|M, D) = \frac{1}{N_t N_o} \sum_{n=1}^{N_o} \sum_{j=1}^{N_t} [u_n^*(t_j) - u_n(t_j, \boldsymbol{\theta})]^2. \tag{2}$$

2.2. Model parameter estimation

For a large number of available data ($N_t N_0$ is large) or for a uniform prior distribution for the model parameters it has been found that the most probable model parameters are obtained by minimizing $J(\boldsymbol{\theta}|M, D)$ over all parameters in Θ that it depends on [13]. Under the previous assumption the posterior probability density function $p(\boldsymbol{\theta}|M, D)$ is in general concentrated in the neighborhood of a lower dimensional manifold in the parameter space. In this context it is useful to classify a Bayesian model class M into one of the three distinct categories: globally identifiable, locally identifiable, and unidentifiable, depending on whether the set of most probable model parameters is a singleton, finite or uncountable, respectively, in the parameter space Θ [13,28,29]. Thus, the problem of estimating the model parameters may be potentially ill-posed, that is, there may be more than one solution. For globally identifiable cases asymptotic approximations of the Bayesian predictive integrals have been used in a number of applications with sufficient accuracy [9,13,14]. In this case the posterior distribution of the model parameters is very peaked and is asymptotically approximated by a multi-dimensional Gaussian distribution centered at the most probable value of the model parameters. When the posterior probability density function is not very peaked or has a flat region, the validity of using asymptotic approximations is doubtful. To avoid these difficulties a simulation-based Bayesian model updating technique is adopted in this study. Such technique, which efficiently generates samples asymptotically distributed as the posterior probability density function, is described in Section 3.

2.3. Model class selection

The Bayesian probabilistic framework can also be used to compare alternative candidate model classes and select the optimal model class based on the available data [16,17,25]. To this end, consider a set $\boldsymbol{M} = \{M^{(1)}, M^{(2)}, \ldots, M^{(n_m)}\}$ of n_m model classes for representing a finite element model. Given data D, the posterior probability of each model class, i.e., $P(M^{(i)}|\boldsymbol{M}, D),\ i = 1, \ldots, n_m$ is

$$P(M^{(i)}|\boldsymbol{M}, D) = \frac{P(D|M^{(i)}) P(M^{(i)}|\boldsymbol{M})}{\sum_{i=1}^{n_m} P(D|M^{(i)}) P(M^{(i)}|\boldsymbol{M})} \tag{3}$$

where $P(M^{(i)}|\boldsymbol{M})$ is the prior probability, and $P(D|M^{(i)})$ is the evidence of the model class $M^{(i)}$. The optimal model class is selected as the one that maximizes $P(M^{(i)}|\boldsymbol{M}, D)$. For the case where no prior information is available the prior probability can be assumed to be equal, that is, $P(M^{(i)}|\boldsymbol{M}) = 1/n_m$. Thus, the selection among the model classes is based solely on their evidence values. The estimation of model class evidences, in the context of a simulation-based approach, is discussed in the following section.

3. Simulation-based approach

3.1. Formulation

An efficient method called transitional Markov chain Monte Carlo is implemented in this work for Bayesian model updating and model class selection [17]. Validation calculations have shown the effectiveness of this approach in a series of practical Bayesian model updating problems [17,30–32]. The method can be applied to a wide range of cases including high-dimensional posterior probability density functions, multimodal distributions, peaked probability density functions, and probability density functions with flat regions. In what follows the basic ideas of the transitional Markov chain Monte Carlo method are briefly discussed. The method iteratively proceeds from the prior to the posterior distribution. It starts with the generation of samples from the prior distribution in order to populate the space in which also the most probable region of the posterior distribution lies. For this purpose a number of non-normalized intermediate distributions $p_j(\boldsymbol{\theta}|M, D),\ j = 1, \ldots, J$, are defined as

$$p_j(\boldsymbol{\theta}|M, D) \propto\ p(D|M, \boldsymbol{\theta})^{\alpha_j}\, p(\boldsymbol{\theta}|M) \tag{4}$$

where the parameter α_j increases monotonically with j such that $\alpha_0 = 0$ and $\alpha_J = 1$. The parameter α_j can be interpreted as the percentage of the total information provided by the dynamic data which is incorporated in the jth iteration of the updating procedure. The first step ($j = 0$) corresponds to the prior distribution and in the last stage ($j = J$) the samples are generated from the posterior distribution. The idea is to choose the values of exponents α_j in such a way that the change of the shape between two adjacent intermediate distributions be small. This small change of the shape makes it possible to efficiently obtain samples from $p_{j+1}(\boldsymbol{\theta}|M, D)$ based on the samples from $p_j(\boldsymbol{\theta}|M, D)$. The value of the parameter α_{j+1} is chosen such that the coefficient of variation for $\{p(D|M, \boldsymbol{\theta}_j^k)^{\alpha_{j+1}-\alpha_j}, k = 1, \ldots, N_j\}$ is equal to some prescribed target value. The upper index $k = 1, \ldots, N_j$ in the previous expression denotes the sample number in the jth iteration step ($\boldsymbol{\theta}_j^k,\ k = 1, \ldots, N_j$).

3.2. Sample generation

Once the parameter α_{j+1} has been determined, the samples are obtained by generating Markov chains where the lead samples are selected from the distribution $p_j(\boldsymbol{\theta}|M, D)$. Each sample of the current stage is generating by applying the Metropolis–Hastings algorithm [33,34]. The lead sample of the Markov chain is a sample from the previous step that is selected according to the probability equal to its normalized weight $\bar{w}(\boldsymbol{\theta}_j^k) = w(\boldsymbol{\theta}_j^k)/\sum_{l=1}^{N_j} w(\boldsymbol{\theta}_j^l)$, where $w(\boldsymbol{\theta}_j^k)$ represents the plausibility weight which is given by $w(\boldsymbol{\theta}_j^k) = p(D|M, \boldsymbol{\theta}_j^k)^{\alpha_{j+1}-\alpha_j}$. The proposal probability density function for the Metropolis–Hastings algorithm is a Gaussian distribution centered at the preceding sample of the chain and with a covariance matrix equal to a scaled version of the estimate covariance matrix of the current intermediate distribution $p_j(\boldsymbol{\theta}|M, D)$. The procedure is repeated until the parameter α_j is equal to 1 ($j = J$). At the last stage the samples ($\boldsymbol{\theta}_J^k,\ k = 1, \ldots, N_J$) are asymptotically distributed as $p(\boldsymbol{\theta}|M, D)$. The previous algorithm also provides an estimate of the evidence for the model class. In fact, it can be shown that the product of the mean of the weights $w(\boldsymbol{\theta}_j^k),\ k = 1, \ldots, N_j$, that is, $1/N_j \sum_{k=1}^{N_j} w(\boldsymbol{\theta}_j^k)$ for all levels ($j = 1, \ldots, J-1$) of the transitional Markov chain Monte Carlo method is an estimator of the evidence which is asymptotically unbiased. For a detailed implementation of the transitional Markov chain Monte Carlo method, including proofs concerning the statistical properties of the estimators the reader is referred to [17].

4. Model reduction technique

4.1. Basic ideas

The proposed Bayesian model updating technique is in general computationally very demanding due to the large number of dynamic finite element analyses required during the updating process. In fact, the model updating technique based on the transitional Markov chain Monte Carlo method involves drawing a large number of samples (of the order of thousands) for populating the important region in the uncertain parameter space. Recall that for each sample generated by the simulation algorithm, a dynamic finite element analysis is needed. This is due to the fact that the

evaluation of each plausibility weight $w(\boldsymbol{\theta}_j^k),\ k = 1, \ldots, N_j,\ j = 0, \ldots, J$, implies the calculation of the likelihood function which requires a dynamic analysis. Consequently, the computational demands may become excessive when the computational time for performing a dynamic finite element analysis is significant. To cope with this difficulty a model reduction technique for linear systems is considered in the present formulation. In particular a method known as substructure coupling or component mode synthesis is implemented here [22,23,35]. Sub-structuring involves dividing the structure into a number of substructures obtaining reduced-order models of the substructures and then assembling a reduced-order model of the entire structure. More specifically, after the division of the structure into substructures the model reduction technique involves two basic steps: definition of sets of substructure modes; and coupling of the substructure-mode models to form a reduced-order system model. In what follows, each of these steps is discussed in detail for the linear components of the structural system.

4.2. Normal and constraint modes

In the present formulation it is assumed that the linear components of the structural model satisfy the equation of motion

$$\mathbf{M}\ddot{\mathbf{u}}(t) + \mathbf{C}\dot{\mathbf{u}}(t) + \mathbf{K}\mathbf{u}(t) = \mathbf{f}(t) \tag{5}$$

where $\mathbf{M}$, $\mathbf{C}$, and $\mathbf{K}$ are the $N \times N$ mass, damping and stiffness matrices of the finite element model, respectively, $\mathbf{u}(t)$ is the vector of dynamic displacements, and $\mathbf{f}(t)$ is the excitation vector. As previously pointed out the first step of the model reduction technique is the definition of sets of substructure modes. In order to define the set of substructure modes the following partitioned form of the mass matrix $\mathbf{M}^s \in R^{n^s \times n^s}$ and stiffness matrix $\mathbf{K}^s \in R^{n^s \times n^s}$ of the substructure s, $s = 1, \ldots, N_s$ is considered

$$\mathbf{M}^s = \begin{bmatrix} \mathbf{M}_{ii}^s & \mathbf{M}_{ib}^s \\ \mathbf{M}_{bi}^s & \mathbf{M}_{bb}^s \end{bmatrix}, \qquad \mathbf{K}^s = \begin{bmatrix} \mathbf{K}_{ii}^s & \mathbf{K}_{ib}^s \\ \mathbf{K}_{bi}^s & \mathbf{K}_{bb}^s \end{bmatrix} \tag{6}$$

where the indices i and b are sets containing the internal and boundary degrees of freedom of the substructure s, respectively. The boundary degrees of freedom include only those that are common with the boundary degrees of freedom of adjacent substructures, while the internal degrees of freedom are not shared with any adjacent substructure. In this framework all boundary coordinates are kept as one set $\mathbf{u}_b^s(t) \in R^{n_b^s}$ and the internal coordinates in the set $\mathbf{u}_i^s(t) \in R^{n_i^s}$. The corresponding equation of motion of the undamped substructure s can be written as

$$\mathbf{M}^s\ddot{\mathbf{u}}^s(t) + \mathbf{K}^s\mathbf{u}^s(t) = \mathbf{f}^s(t) \tag{7}$$

where $\mathbf{u}^s(t)^T = \langle \mathbf{u}_i^s(t)^T, \mathbf{u}_b^s(t)^T \rangle \in R^{n^s}$ is the displacement vector (physical coordinates) of dimension $n^s = n_i^s + n_b^s$ and the vector $\mathbf{f}^s(t)$ contains the externally applied forces as well as the reaction forces on the substructure due to its connection to adjacent substructures at boundary degrees of freedom.

4.2.1. Fixed-interface normal modes

The normal modes are eigenvectors and can be classified according to the interface boundary conditions specified for the substructure [22]. Specifically, the fixed-interface normal modes are obtained by restraining all boundary degrees of freedom and solving the eigenproblem

$$\mathbf{K}_{ii}^s \boldsymbol{\Phi}_{ii}^s = \mathbf{M}_{ii}^s \boldsymbol{\Phi}_{ii}^s \boldsymbol{\Lambda}_{ii}^s \tag{8}$$

where the matrix $\boldsymbol{\Phi}_{ii}^s$ contains the complete set of n_i^s fixed-interface normal modes, and $\boldsymbol{\Lambda}_{ii}^s$ is the corresponding matrix containing the eigenvalues. The fixed-interface normal modes are normalized with respect to the mass matrix $\mathbf{M}_{ii}^s$ and stiffness matrix $\mathbf{K}_{ii}^s$ satisfying ${\boldsymbol{\Phi}_{ii}^s}^T \mathbf{M}_{ii}^s \boldsymbol{\Phi}_{ii}^s = \mathbf{I}_{ii}^s$ and ${\boldsymbol{\Phi}_{ii}^s}^T \mathbf{K}_{ii}^s \boldsymbol{\Phi}_{ii}^s = \boldsymbol{\Lambda}_{ii}^s$.

4.2.2. Interface constraint modes

On the other hand the constraint modes are defined as the static deformation of a structure when a unit displacement is applied to one coordinate of a specified set of constraint coordinates while the remaining coordinates of that set are restrained, and the remaining degrees of freedom of the structure are force-free [22]. In this context the interface

constraint modes are obtained by setting a unit displacement on the boundary coordinates $\mathbf{u}_b^s(t)$ and zero forces in the internal degrees of freedom. The set of modes is given by

$$\begin{bmatrix} \mathbf{K}_{ii}^s & \mathbf{K}_{ib}^s \\ \mathbf{K}_{bi}^s & \mathbf{K}_{bb}^s \end{bmatrix} \begin{bmatrix} \boldsymbol{\Psi}_{ib}^s \\ \mathbf{I}_{bb}^s \end{bmatrix} = \begin{bmatrix} \mathbf{0}_{ib}^s \\ \mathbf{R}_{bb}^s \end{bmatrix} \tag{9}$$

from where the interface constraint-mode matrix $\boldsymbol{\Psi}_c^s$ is defined as

$$\boldsymbol{\Psi}_c^s = \begin{bmatrix} \boldsymbol{\Psi}_{ib}^s \\ \mathbf{I}_{bb}^s \end{bmatrix} = \begin{bmatrix} -\mathbf{K}_{ii}^{s\,-1} \mathbf{K}_{ib}^s \\ \mathbf{I}_{bb}^s \end{bmatrix} \tag{10}$$

where $\boldsymbol{\Psi}_{ib}^s \in R^{n_i^s \times n_b^s}$ is the interior partition of the constraint-mode matrix. Based on the previous fixed-interface and constraint modes, a displacement transformation matrix is defined in the following section to introduce a set of generalized coordinates.

4.3. Craig–Bampton method

The displacement transformation of the Craig–Bampton method [22,35] employs a combination of fixed-interface normal modes and interface constraint modes, and takes the form

$$\mathbf{u}^s(t) = \begin{Bmatrix} \mathbf{u}_i^s(t) \\ \mathbf{u}_b^s(t) \end{Bmatrix} = \begin{bmatrix} \boldsymbol{\Phi}_{ik}^s & \boldsymbol{\Psi}_{ib}^s \\ \mathbf{0}_{bk}^s & \mathbf{I}_{bb}^s \end{bmatrix} \begin{Bmatrix} \mathbf{v}_k^s(t) \\ \mathbf{v}_b^s(t) \end{Bmatrix} = \boldsymbol{\Psi}^s \ \ \mathbf{v}^s(t) \tag{11}$$

where $\boldsymbol{\Phi}_{ik}^s \in R^{n_i^s \times n_{ik}^s}$ is the interior partition of the matrix $\boldsymbol{\Phi}_{ii}^s$ of the n_{ik}^s kept fixed-interface normal modes ($n_{ik}^s \leq n_i^s$), $\mathbf{v}^s(t)$ represents the substructure generalized coordinates composed by the modal coordinates $\mathbf{v}_k^s(t)$ of the kept fixed-interface normal modes and the boundary coordinates $\mathbf{v}_b^s(t) = \mathbf{u}_b^s(t)$, $\boldsymbol{\Psi}^s \in R^{n^s \times \hat{n}^s}$ is the Craig–Bampton transformation matrix with $\hat{n}^s = n_{ik}^s + n_b^s$ and all other terms have been previously defined. The substructure mass matrix $\hat{\mathbf{M}}^s \in R^{\hat{n}^s \times \hat{n}^s}$ and stiffness matrix $\hat{\mathbf{K}}^s \in R^{\hat{n}^s \times \hat{n}^s}$ in generalized coordinates $\mathbf{v}^s(t)$ are given by

$$\hat{\mathbf{M}}^s = \boldsymbol{\Psi}^{s\,T} \mathbf{M}^s \boldsymbol{\Psi}^s, \qquad \hat{\mathbf{K}}^s = \boldsymbol{\Psi}^{s\,T} \mathbf{K}^s \boldsymbol{\Psi}^s. \tag{12}$$

Next, the vector of generalized coordinates for all the N_s substructures

$$\mathbf{v}(t)^T = \langle \mathbf{v}^1(t)^T, \ldots, \mathbf{v}^{N_s}(t)^T \rangle \in R^{n_v} \tag{13}$$

where $n_v = \sum_{s=1}^{N_s} \hat{n}^s$ is introduced. Based on this vector, a new vector $\mathbf{q}(t)$ that contains the independent generalized coordinates consisting of the fixed-interface modal coordinates $\mathbf{v}_k^s(t)$ for each substructure and the physical coordinates $\mathbf{v}_b^l(t), l = 1, \ldots, N_b$ at the N_b interfaces is defined as

$$\mathbf{q}(t)^T = \langle \mathbf{v}_k^1(t)^T, \ldots, \mathbf{v}_k^{N_s}(t)^T, \mathbf{v}_b^1(t)^T, \ldots, \mathbf{v}_b^{N_b}(t)^T \rangle \in R^{n_q} \tag{14}$$

where $n_q = \sum_{s=1}^{N_s} n_{ik}^s + \sum_{l=1}^{N_b} n_b^l$, and n_b^l is the number of degrees of freedom at the interface l ($l = 1, \ldots, N_b$). These two vectors are related by the transformation

$$\mathbf{v}(t) = \mathbf{T}\mathbf{q}(t) \tag{15}$$

where the matrix $\mathbf{T} \in R^{n_v \times n_q}$ is a matrix of zeros and ones that couples the independent generalized coordinates $\mathbf{q}(t)$ of the reduced system with the generalized coordinates of each substructure. The assembled mass matrix $\hat{\mathbf{M}} \in R^{n_q \times n_q}$ and the stiffness matrix $\hat{\mathbf{K}} \in R^{n_q \times n_q}$ for the independent reduced set $\mathbf{q}(t)$ of generalized coordinates take the form

$$\hat{\mathbf{M}} = \mathbf{T}^T \begin{bmatrix} \hat{\mathbf{M}}^1 & \mathbf{0} & \mathbf{0} \\ \mathbf{0} & \ddots & \mathbf{0} \\ \mathbf{0} & \mathbf{0} & \hat{\mathbf{M}}^{N_s} \end{bmatrix} \mathbf{T}, \qquad \hat{\mathbf{K}} = \mathbf{T}^T \begin{bmatrix} \hat{\mathbf{K}}^1 & \mathbf{0} & \mathbf{0} \\ \mathbf{0} & \ddots & \mathbf{0} \\ \mathbf{0} & \mathbf{0} & \hat{\mathbf{K}}^{N_s} \end{bmatrix} \mathbf{T} \tag{16}$$

where the matrices $\hat{\mathbf{M}}^s$ and $\hat{\mathbf{K}}^s$, $s = 1, \ldots, N_s$ are given in Eq. (12). Note that the vectors $\mathbf{v}(t)$ and $\mathbf{q}(t)$ do not contain internal degrees of freedom. They contain fixed-interface modal coordinates and physical coordinates at the interfaces.

The number of fixed-interface normal modes to be used in the reduced-order model can be established by using different criteria. In particular, a criterion based on the agreement between modal frequencies obtained from the complete finite element model and the ones computed from the reduced model is implemented in the present formulation. The specific implementation is discussed in detail in Section 6 (Numerical Examples).

It is noted that the number of interface degrees of freedom involved in the transformation (15) may become very large specially for three dimensional finite element models. In this regard further reduction in the generalized coordinates can be achieved by replacing the interface degrees of freedom by a reduced number of interface modes. This particular feature of the model reduction technique is not considered in the present formulation. The reader is referred to [23,36] for a detailed description on how to define a reduced set of interface degrees of freedom.

4.4. Dynamic response

The dynamic response of the finite element model of the original unreduced system is obtained by the modal solution in the present implementation. In this approach it is assumed that the response can be represented by a linear combination of the mode shapes as

$$\mathbf{u}(t) = \sum_{r=1}^{m} \boldsymbol{\upsilon}_r \eta_r(t) = \boldsymbol{\Upsilon}\boldsymbol{\eta}(t) \tag{17}$$

where $\mathbf{u}(t)$ is the displacement vector of the original structure, m is the number of modes considered, $\eta_r(t), r = 1, \ldots, m$ are the modal responses, $\boldsymbol{\upsilon}_r \in R^N, r = 1, \ldots, m$ are the eigenvectors associated with the eigenproblem of the undamped equation of motion of the original system, $\boldsymbol{\Upsilon}$ is the matrix of mode shapes, and $\boldsymbol{\eta}(t)$ is the vector of modal response functions. For classically damped systems the modal responses satisfy the differential equation

$$\ddot{\eta_r}(t) + 2\xi_r\omega_r\dot{\eta_r}(t) + \omega_r^2\eta_r(t) = \boldsymbol{\upsilon}_r^T\mathbf{f}(t), \quad r = 1, \ldots, m \tag{18}$$

where $\omega_r, r = 1, \ldots, m$ are the natural frequencies of the system, $\xi_r, r = 1, \ldots, m$ are the corresponding damping ratios, and $\mathbf{f}(t)$ is the force vector applied on the original system. In the previous modal equations it has been assumed that the eigenvectors are normalized with respect to the system mass matrix. The solution for the modal responses can be obtained by any suitable step-by-step integration scheme [37]. The natural frequencies $\omega_r, r = 1, \ldots, m$ are obtained by solving the eigenproblem of the reduced-order system model

$$(\hat{\mathbf{K}} - \omega_r^2\hat{\mathbf{M}})\boldsymbol{\upsilon}_{pr} = \mathbf{0}, \quad r = 1, \ldots, m \tag{19}$$

where $\boldsymbol{\upsilon}_{pr}, r = 1, \ldots, m$ are the mode shapes of the reduced-order system. Introducing a constant matrix $\bar{\mathbf{T}} \in R^{N\times n_u}$ ($n_u = \sum_{s=1}^{N_s} n^s$) to map the vector $\bar{\mathbf{u}}(t)^T = \langle \mathbf{u}^1(t)^T, \ldots, \mathbf{u}^{N_s}(t)^T \rangle \in R^{n_u}$ of the physical coordinates for all substructures to the independent physical coordinates $\mathbf{u}(t)$ of the original unreduced system, the physical mode shapes $\boldsymbol{\upsilon}_r$ of the structure can be recovered from the mode shapes $\boldsymbol{\upsilon}_{pr}$ as $\boldsymbol{\upsilon}_r = \bar{\mathbf{T}}\boldsymbol{\Psi}\mathbf{T}\boldsymbol{\upsilon}_{pr}$ where the matrix $\boldsymbol{\Psi} \in R^{n_u\times n_v}$ is a block diagonal matrix defined in terms the Craig–Bampton transformation matrices of all substructures, that is, $\boldsymbol{\Psi} = blockdiag(\boldsymbol{\Psi}^1, \ldots, \boldsymbol{\Psi}^{N_s})$. It is noted that the previous representation of the solution for the original finite element model can be extended in a straightforward manner for the general case of non-classically damped systems. In those cases the equation of motion is recast into a first-order $2N$ state-space form, and the solution is represented as a linear combination of complex mode shapes [38,39].

5. Model updating based on the reduced system

5.1. Problem formulation

In the present formulation it is assumed that the stiffness matrix of the original system depends linearly on the model parameters $\boldsymbol{\theta}$ and that the mass matrix is constant, independent of $\boldsymbol{\theta}$. It is noted that this case is often encountered in many practical applications such as model updating, structural optimization and damage detection techniques. This linear dependence implies that at the substructure level the stiffness matrix as well as its partitions admit a similar characterization. In particular the following two cases are considered here. In the first case it is assumed that the stiffness matrix of a substructure s does not depend on the model parameters. In this case the stiffness matrix is

written as $\mathbf{K}^s = \mathbf{K}^s_0$. The corresponding normal and constraint modes are computed once for that substructures. In the second case it is assumed that the stiffness matrix of a substructure s depends only on one model parameter, say θ_j (jth component of $\boldsymbol{\theta}$). Specifically, let S_j be the set of substructures that depends on θ_j. Then the stiffness matrix of a substructure $s \in S_j$ can be written as $\mathbf{K}^s = \bar{\mathbf{K}}^s\theta_j$, where the matrix $\bar{\mathbf{K}}^s$ is independent of θ_j. Of course the partitions of the stiffness matrix $\mathbf{K}^s$ admit the same parametrization (see Eq. (6)). From this representation it is easy to show that the eigenvalues and eigenvectors associated with the fixed-interface normal modes are given by $\boldsymbol{\Lambda}^s_{ii} = \bar{\boldsymbol{\Lambda}}^s_{ii}\theta_j$ and $\boldsymbol{\Phi}^s_{ii} = \bar{\boldsymbol{\Phi}}^s_{ii}$ where the matrices $\bar{\boldsymbol{\Lambda}}^s_{ii}$ and $\bar{\boldsymbol{\Phi}}^s_{ii}$ are the solutions of the eigenproblem

$$\bar{\mathbf{K}}^s_{ii}\bar{\boldsymbol{\Phi}}^s_{ii} = \mathbf{M}^s_{ii}\bar{\boldsymbol{\Phi}}^s_{ii}\bar{\boldsymbol{\Lambda}}^s_{ii} \tag{20}$$

where the matrices $\bar{\boldsymbol{\Phi}}^s_{ii}$ and $\bar{\boldsymbol{\Lambda}}^s_{ii}$ are independent of θ_j. In addition, the interface constraint modes are also independent of θ_j since $\boldsymbol{\Psi}^s_{ib} = -\mathbf{K}^{s\,-1}_{ii}\mathbf{K}^s_{ib} = -\bar{\mathbf{K}}^{s\,-1}_{ii}\bar{\mathbf{K}}^s_{ib}$. Therefore a single substructure analysis is required to provide the exact estimate of the normal and constraint modes for any value of the modal parameter θ_j. This is a very important result since the computationally intensive re-analyses for estimating the normal modes of each substructure for different values of θ_j involved in the identification procedure are completely avoided.

5.2. Reduced stiffness matrix

Based on the previous results it is simple to verify that the reduced stiffness matrix of the substructure s, considering the full set of interface degrees of freedom, takes the form $\hat{\mathbf{K}}^s = \hat{\bar{\mathbf{K}}}^s\theta_j$ where $\hat{\bar{\mathbf{K}}}^s = \boldsymbol{\Psi}^{s\,T}\bar{\mathbf{K}}^s\boldsymbol{\Psi}^s$. Thus, the reduced matrix $\hat{\bar{\mathbf{K}}}^s$ is a constant matrix independent of the model parameters $\boldsymbol{\theta}$. Consequently the stiffness matrix of the Craig–Bampton reduced system can be written as

$$\hat{\mathbf{K}} = \hat{\mathbf{K}}_0 + \sum_{j=1}^{N_\theta}\hat{\bar{\mathbf{K}}}_j\theta_j \tag{21}$$

where N_θ is the number of independent model parameters and the matrices $\hat{\mathbf{K}}_0$ and $\hat{\bar{\mathbf{K}}}_j,\ j = 1,\ldots,N_\theta$ are defined as

$$\hat{\mathbf{K}}_0 = \mathbf{T}^T\begin{bmatrix}\hat{\mathbf{K}}^1_0\delta_{10} & \mathbf{0} & \mathbf{0}\\ \mathbf{0} & \ddots & \mathbf{0}\\ \mathbf{0} & \mathbf{0} & \hat{\mathbf{K}}^{N_s}_0\delta_{N_s0}\end{bmatrix}\mathbf{T}, \qquad \hat{\bar{\mathbf{K}}}_j = \mathbf{T}^T\begin{bmatrix}\hat{\bar{\mathbf{K}}}^1\delta_{1j} & \mathbf{0} & \mathbf{0}\\ \mathbf{0} & \ddots & \mathbf{0}\\ \mathbf{0} & \mathbf{0} & \hat{\bar{\mathbf{K}}}^{N_s}\delta_{N_sj}\end{bmatrix}\mathbf{T} \tag{22}$$

where $\delta_{s0} = 1$ if the substructure s does not depend on the model parameters $\boldsymbol{\theta}$ and $\delta_{s0} = 0$ otherwise, $\delta_{sj} = 1$ if the substructure s depends on the parameter θ_j and $\delta_{sj} = 0$ otherwise, and all other terms have been previously defined. Note that the assembled matrices $\hat{\bar{\mathbf{K}}}_j,\ j = 1,\ldots,N_\theta$ are independent of the value of $\boldsymbol{\theta}$ and therefore these matrices are computed and assembled once. This results in substantial savings since there is no need to re-compute and re-assemble these matrices during the identification process.

5.3. Final remarks

It is stressed that the efficiency of the above formulation in terms of the number of substructure analyses required is based on the assumption that the stiffness matrix of the substructures depend only on one model parameter. For a more general case, the normal and constraint modes have to be recomputed in each iteration of the identification process. Some guidelines on how to proceed in a more efficient manner for the general case are indicated in the Conclusions section. In summary, the assembled matrices $\hat{\mathbf{K}}_0$ and $\hat{\bar{\mathbf{K}}}_j,\ j = 1,\ldots,N_\theta$ involved in the reduced system are computed once and therefore there is no need to perform re-analyses of each substructure during the identification process. Of course, the eigenproblem of the reduced order system model (Eq. (19)) needs to be solved for different values of $\boldsymbol{\theta}$ in order to compute the corresponding dynamic response of the original unreduced system.

Finally, it is noted that the previous formulation can be extended in a direct manner to linear models with localized nonlinearities. In these cases the model reduction technique is used to obtain reduced-order models of the linear substructures. These reduced-order models together with the nonlinear substructures are assembled in order to form

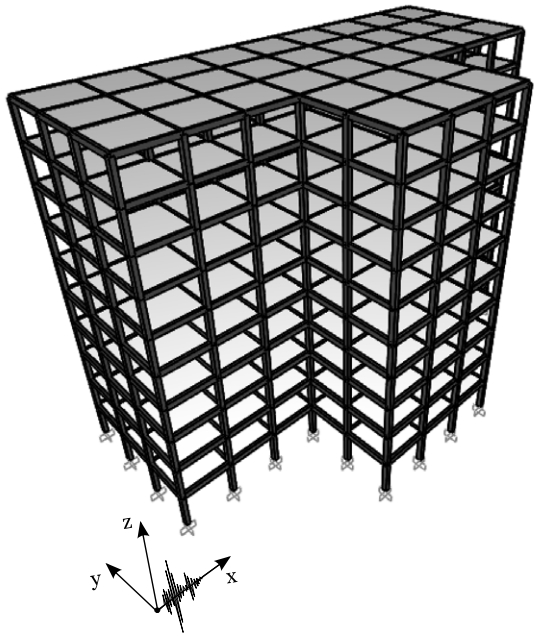

Fig. 1. Isometric view of the finite element model.

a reduced-order model for the entire structure. This procedure is illustrated in the following section (example 2) for one particular class of problems. Some comments regarding the generalization of the methodology to different class of problems and different types of localized nonlinearities are presented in the Conclusions section.

6. Numerical examples

Two example problems are considered in this section. The first application deals with a linear system while the second application considers a linear model with localized nonlinearities. The objective of the first example is to evaluate the effectiveness of the proposed model reduction technique in a linear model identification problem. On the other hand, the goal of the second application is to evaluate the performance of the proposed technique in a nonlinear model updating problem that considers a base-isolated structural system.

6.1. Example 1: updating of linear model

6.1.1. Model description

The structural system shown in Fig. 1 is considered in this example. It consists of a ten floors three-dimensional reinforced concrete building model. Material properties of the reinforced concrete structure have been assumed as follows: Young's modulus $E = 2.34 \times 10^{10}$ N/m^2; Poisson's ratio $\nu = 0.3$; and mass density $\rho = 2500$ kg/m^3. The height of each floor is 3.5 m leading to a total height of 35.0 m for the structure. The floors are modeled with shell elements with a thickness of 0.3 m and beam elements of rectangular cross section of dimension 0.3 m $\times$ 0.6 m from floors 1 to 5 and 0.25 m $\times$ 0.5 m from floors 6 to 10. Each floor is supported by 48 columns of rectangular cross section of dimension 0.8 m $\times$ 0.9 m. The corresponding finite element model, denoted herein as reference model, has approximately 40,000 degrees of freedom. A 2% of critical damping for the modal damping ratios is introduced in the model.

6.1.2. Identification problem

For the identification problem the structure is divided into a number of substructures and it is assumed that a stiffness reduction is concentrated in one or more substructures producing changes in the stiffness characteristics of those substructures. In particular the structural model is subdivided into six substructures as shown in Fig. 2. Substructures 1, 3 and 5 are composed by the column elements of the first, second and third floor, respectively. Substructures 2 and 4 correspond to the slabs and beam elements of the first and second floor, respectively, and substructure 6 contains the upper floors structural components (columns, beams and slabs). For illustration purposes three model classes

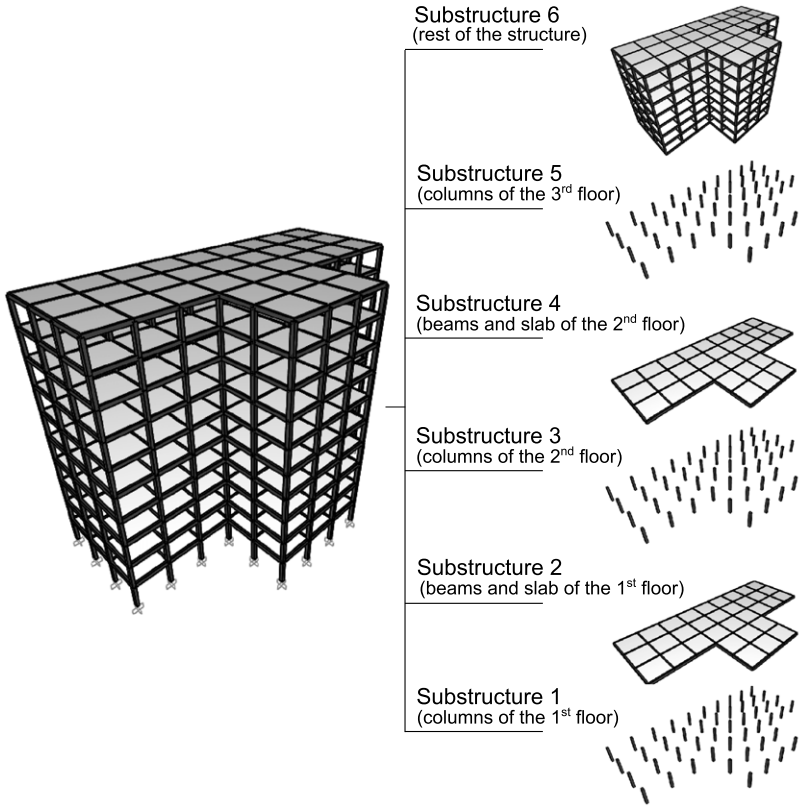

Fig. 2. Substructures of the finite element model used for identification.

$M^{(i)},\ i = 1, 2, 3$ are introduced to monitor the updated process, which is defined in terms of a stiffness reduction of 20% of the nominal stiffness value in the x direction of the columns of the first floor. Model class $M^{(1)}$ contains one parameter (θ_1) related to the stiffness of the columns of the first floor. On the other hand, model class $M^{(2)}$ contains two parameters (θ_2, θ_3) associated with the stiffness of the columns of the first and second floor, respectively. Finally, model class $M^{(3)}$ contains three parameters ($\theta_4, \theta_5, \theta_6$) associated with the stiffness of the columns of the first, second and third floor, respectively. Note that the model class $M^{(2)}$ can monitor changes associated with the stiffness reduction in either substructures 1 and 3. Likewise model class $M^{(3)}$ can monitor changes associated with the stiffness reduction in substructures 1, 3 and 5.

6.1.3. Simulated response data

The identification process is based on simulated data. To this end the original unreduced finite element model is excited horizontally (in the x direction) with the Santa Lucia ground-motion record recorded during the 2010 Chilean earthquake. The input ground acceleration time history is shown in Fig. 3. It corresponds to a ground motion of moderate intensity. The measured responses are simulated by first calculating the acceleration response in the x direction at floors 1, 2, 3 and 4 of the original structure with a stiffness reduction of 20% (in the x direction) of the columns of the first floor. Then, a Gaussian discrete white noise sequence with standard deviation equal to 10% of the root-mean square value of the corresponding acceleration time histories is added. The responses are computed at the center of mass of the floors. One hundred seconds of data with sampling interval $\Delta t = 0.05$ s are used, given a total of $N_t = 2000$ data points. The simulated responses provide the data for the identification process. Simulated accelerations are plotted in Fig. 4 for the first four floors.

6.1.4. Reduced model

The effectiveness of the model reduction technique for the specific problem considered in this example is investigated in this section. For each substructure it is selected to retain all fixed-interface normal modes that have

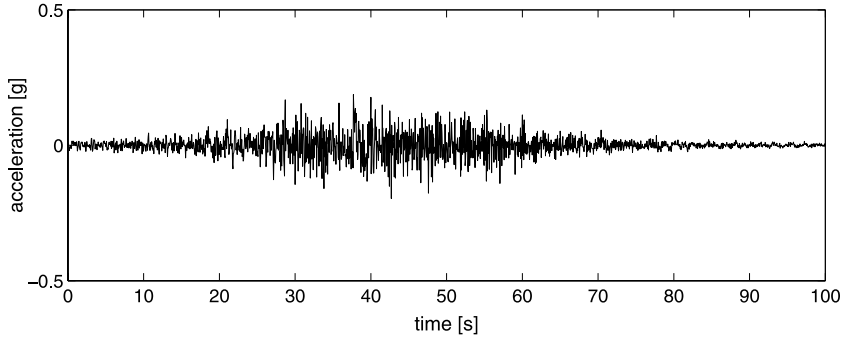

Fig. 3. Santa Lucia ground-motion record (2010 Chilean earthquake).

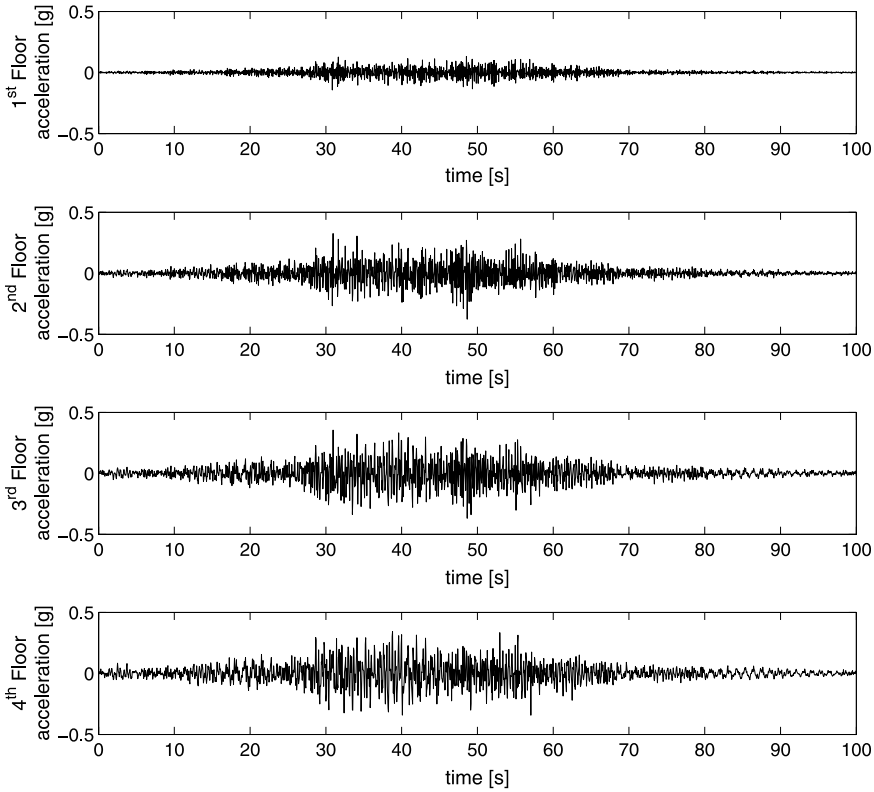

Fig. 4. Simulated acceleration time histories.

frequency less than $\omega_{\max} = \alpha\omega_c$, where α is a multiplication factor and ω_c is a cut-off frequency. The cut-off frequency is selected to be the 12th modal frequency of the reference finite element model. Table 1 shows the fractional error (in percentage) between the modal frequencies using the complete finite element model and the modal frequencies computed using the reduced model as a function of the number of fixed-interface normal modes. Representative values of α for substructures 1, 3 and 5 range from 18 to 20, from 4 to 6 for substructures 2 and 4, and from 1 to 5 for substructure 6. The different ranges are due to the fact that the spectral properties of the substructures are quite different. For example the lowest frequencies corresponding to substructures 1, 3 and 5 are substantially higher than the lowest frequencies of substructures 2 and 4. Three scenarios, which are defined in Table 2, are considered in Table 1. It is observed that the fractional errors are quite small for scenarios No. 2 and No. 3. In fact, the fractional error for the lowest 12 modes fall below 0.1% for both scenarios. Contrarily, an error up to almost 4% for the 12th modal frequency is obtained for scenario No. 1. Based on the results of Table 1 the reduced-order model obtained

Table 1
Fractional modal frequency error between the modal frequencies of the full model and the reduced model for different scenarios. Full set of interface degrees of freedom case.

Frequency number	ω (full FEM) (rad/s)	Fractional error (%)		
		Scenario no. 1	Scenario no. 2	Scenario no. 3
1	5.7817	1.828×10^{-3}	1.634×10^{-4}	3.174×10^{-5}
2	5.8213	2.229×10^{-3}	5.944×10^{-5}	3.436×10^{-5}
3	6.0658	9.933×10^{-3}	1.638×10^{-4}	5.345×10^{-5}
4	17.0956	1.080×10^{-1}	3.175×10^{-3}	1.974×10^{-3}
5	17.3154	9.864×10^{-2}	9.086×10^{-3}	2.005×10^{-3}
6	18.0777	5.416×10^{-1}	8.993×10^{-3}	3.105×10^{-3}
7	32.2909	3.447×10^{-1}	1.487×10^{-2}	1.102×10^{-2}
8	33.3774	3.415×10^{-1}	3.738×10^{-2}	1.204×10^{-2}
9	34.8733	2.436×10^{0}	3.751×10^{-2}	1.584×10^{-2}
10	49.7860	3.441×10^{-2}	2.295×10^{-2}	2.225×10^{-2}
11	52.4705	5.287×10^{-2}	3.207×10^{-2}	2.565×10^{-2}
12	54.9341	3.962×10^{1}	3.423×10^{-2}	2.585×10^{-2}

Table 2
Number of fixed-interface normal modes (Internal-DOF) per substructures and total number of fixed-interface normal modes for different scenarios.

Substructure	Scenario no. 1		Scenario no. 2		Scenario no. 3	
	α	Internal-DOF	α	Internal-DOF	α	Internal-DOF
1	$\alpha = 18$	48	$\alpha = 18$	48	$\alpha = 19$	96
2	$\alpha = 4$	33	$\alpha = 4$	33	$\alpha = 5$	40
3	$\alpha = 18$	48	$\alpha = 18$	48	$\alpha = 19$	96
4	$\alpha = 4$	33	$\alpha = 4$	33	$\alpha = 5$	40
5	$\alpha = 18$	48	$\alpha = 18$	48	$\alpha = 19$	96
6	$\alpha = 1$	8	$\alpha = 3$	155	$\alpha = 4$	340
Total Internal-DOF		218		365		708
Total interface degrees of freedom				864		

with scenario No. 2, in terms of the number of fixed-interface normal modes, is considered for the identification process. The comparison with the lowest 12 modes seems to be reasonable since validation calculations show that the contribution of the higher order modes (higher than the 12th mode) in the dynamic response of the model is negligible.

Then, a total of 365 generalized coordinates, corresponding to the fixed-interface normal modes, out of approximately 39,136 degrees of freedom (DOF) of the original model are retained for all six substructures as shown in Table 2. Thus, about two orders of magnitude reduction in the number of interior degrees of freedom is achieved in this case. It is important to note that the selection of the fixed-interface modes per substructure, necessary to achieve a prescribed accuracy, can be done off-line, before the identification procedure takes place. On the other hand it is seen that the total number of interface degrees of freedom is equal to 864. In conclusion, the number of degrees of freedom of the reduced model, corresponding to scenario No. 2, considering the full set of interface degrees of freedom is 1229 ($n_q = 1229$ in relation to the general formulation). A further reduction in the number of generalized coordinates may be achieved by replacing the interface degrees of freedom by a reduced number of interface modes. It turns out that a large percentage of interface modes needs to be retained in order to obtain a small fractional error for the lowest 12 modes in this case (of the order of 0.1%). This is reasonable since a relatively small number of column elements support each floor. Consequently all interface degrees of freedom are retained in the reduced-order model. In spite of this fact a significant reduction in the number of generalized coordinates is obtained with respect to the number of the degrees of freedom of the original unreduced finite element model. In fact, an almost 97% reduction is obtained in this application. Finally, it is noted that the model classes $M^{(i)},\ i = 1, 2, 3$ previously defined are characterized from the unchanged or nominal structure ($\theta_i = 1,\ i = 1, 2, 3, 4, 5, 6$) corresponding to this reduced-order model.

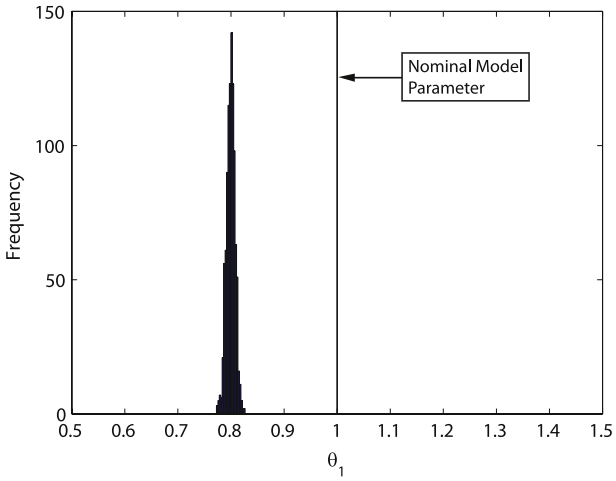

Fig. 5. Posterior histogram of model parameter θ_1 for model class $M^{(1)}$. Mean estimate: $\bar{\theta}_1 = 0.80$.

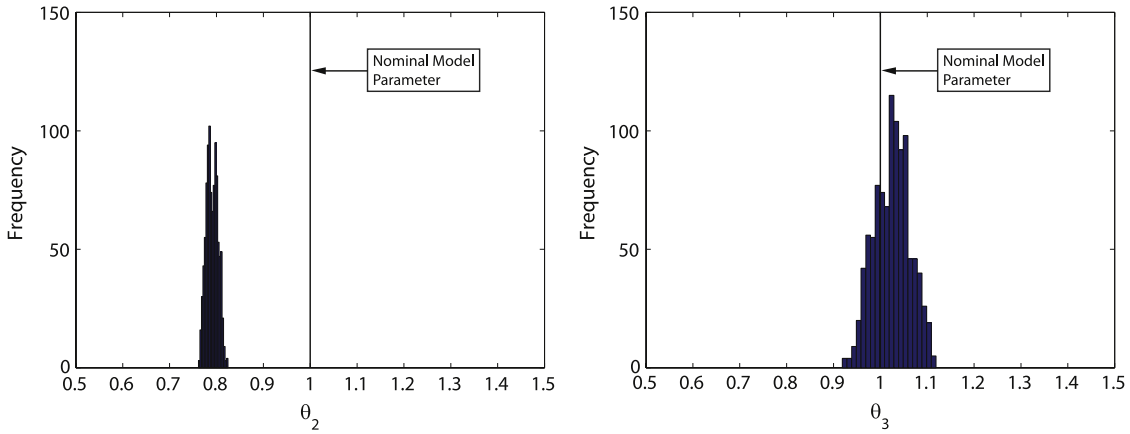

Fig. 6. Posterior histograms of model parameters θ_2 and θ_3 for model class $M^{(2)}$. Mean estimates: $\bar{\theta}_2 = 0.79$, $\bar{\theta}_3 = 1.03$.

6.1.5. Results of identification process

The model updating is performed using the transitional Markov chain Monte Carlo method [17] with 1000 samples per stage. The prior probability density function for the model parameters $\theta_i,\ i = 1, 2, 3, 4, 5, 6$ are independent uniform distributions defined over the interval [0.5, 1.5]. The reference structure (unchanged) is characterized in terms of the model parameters with values equal to one, i.e. $\theta_i = 1,\ i = 1, 2, 3, 4, 5, 6$. Figs. 5–7 show the histograms defined by the posterior samples of the model parameters corresponding to model classes $M^{(i)},\ i = 1, 2, 3$. In addition, the value of the nominal system parameters are also indicated in the figures.

It is seen that the agreement between the actual system and the model characterized by the posterior samples is excellent for model class $M^{(1)}$. The model parameter θ_1 is distributed around the actual value $\theta_1 = 0.8$. In fact the mean estimate of this parameter is equal to $\bar{\theta}_1 = 0.80$. Similar results are obtained for model classes $M^{(2)}$ and $M^{(3)}$. That is, these model classes are able to identify the stiffness reduction of the columns of the first floor. Actually the mean value of the model parameters θ_2 and θ_4 is equal to 0.79. These results are reasonable since model classes $M^{(2)}$ and $M^{(3)}$ also monitor the stiffness of the substructure that contains the actual change (substructure 1). On the other hand it is observed that the parameters related to the stiffness of the columns of the second and the third floor are distributed around their actual values $\theta_3 = \theta_5 = \theta_6 = 1.0$. This is consequent since the stiffnesses of these columns are unchanged. To get insight into the identification process, Fig. 8 shows how the samples in the (θ_2–θ_3) space converge for model class $M^{(2)}$. From the different steps of the transitional Markov chain Monte Carlo method it is observed that the data is strongly correlated along a certain direction in the parameter space. Such correlation shows that an

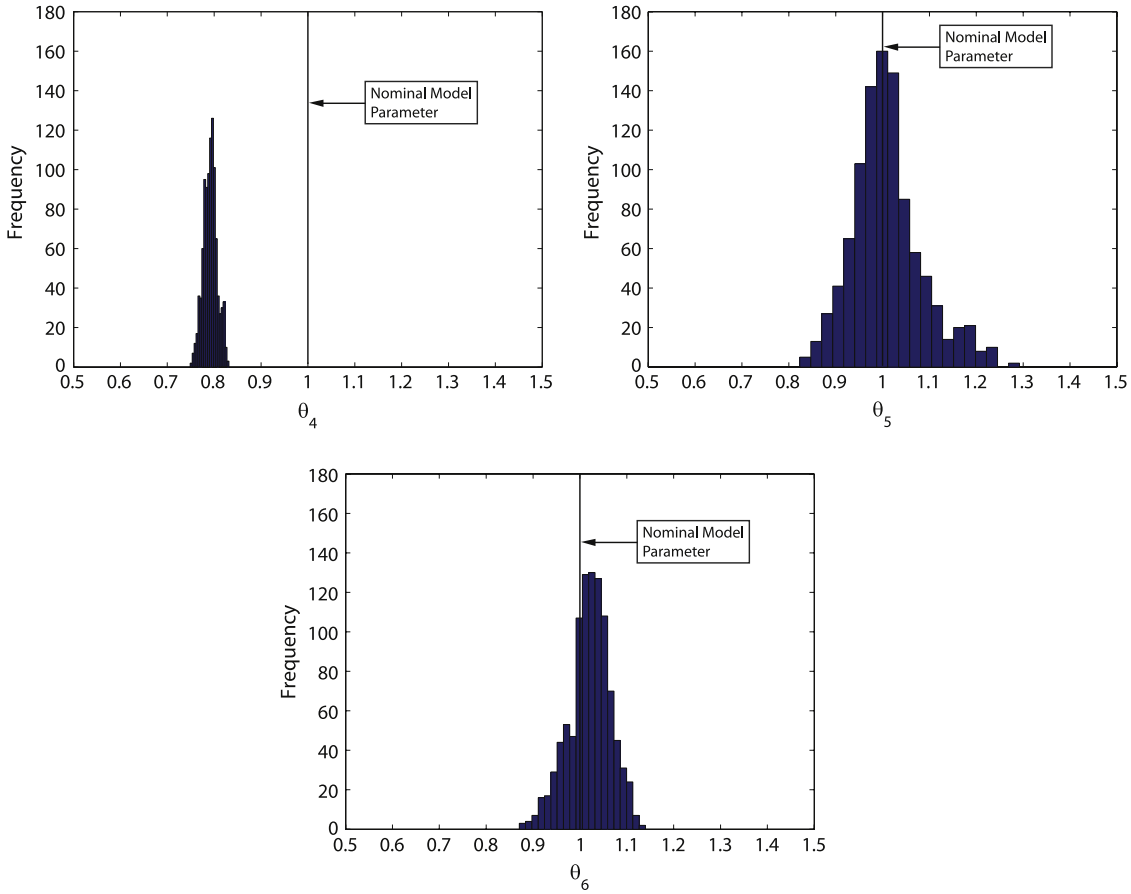

Fig. 7. Posterior histograms of model parameters θ_4, θ_5 and θ_6 for model class $M^{(3)}$. Mean estimates: $\bar{\theta}_4 = 0.79, \bar{\theta}_5 = 1.01, \bar{\theta}_6 = 1.02$.

Table 3
Bayesian model class selection results.

Model class	Log evidence
$M^{(1)}$	−335
$M^{(2)}$	−425
$M^{(3)}$	−576

increase in the stiffness of the columns of the first floor is compensated by a decrease in the stiffness of the columns of the second floor during the identification process, which is reasonable from a structural point of view. Thus, all points along that direction correspond to structural models that have almost the same response at the measured degrees of freedom. In summary, the predictive capabilities of the identification methodology are not compromised by the use of the reduced-order model.

The issue of model class selection is next explored. Results of Bayesian model class selection are shown in Table 3. The evidence clearly favor model class $M^{(1)}$, which is unsurprising as it contains the parameterized substructure with actual change in the stiffness properties (substructure 1). Note that model classes $M^{(2)}$ and $M^{(3)}$ also contains the parameterized substructure 1. However, among all model classes the proposed updating methodology favor the model class $M^{(1)}$ with the least number of parameters which is consistent with theoretical results for model class penalization for over parametrization available for Bayesian model class selection [25,40]. This result is clear by comparing the evidence of model classes $M^{(2)}$ and $M^{(3)}$. Thus, model classes $M^{(2)}$ and $M^{(3)}$ are not favored by the proposed methodology.

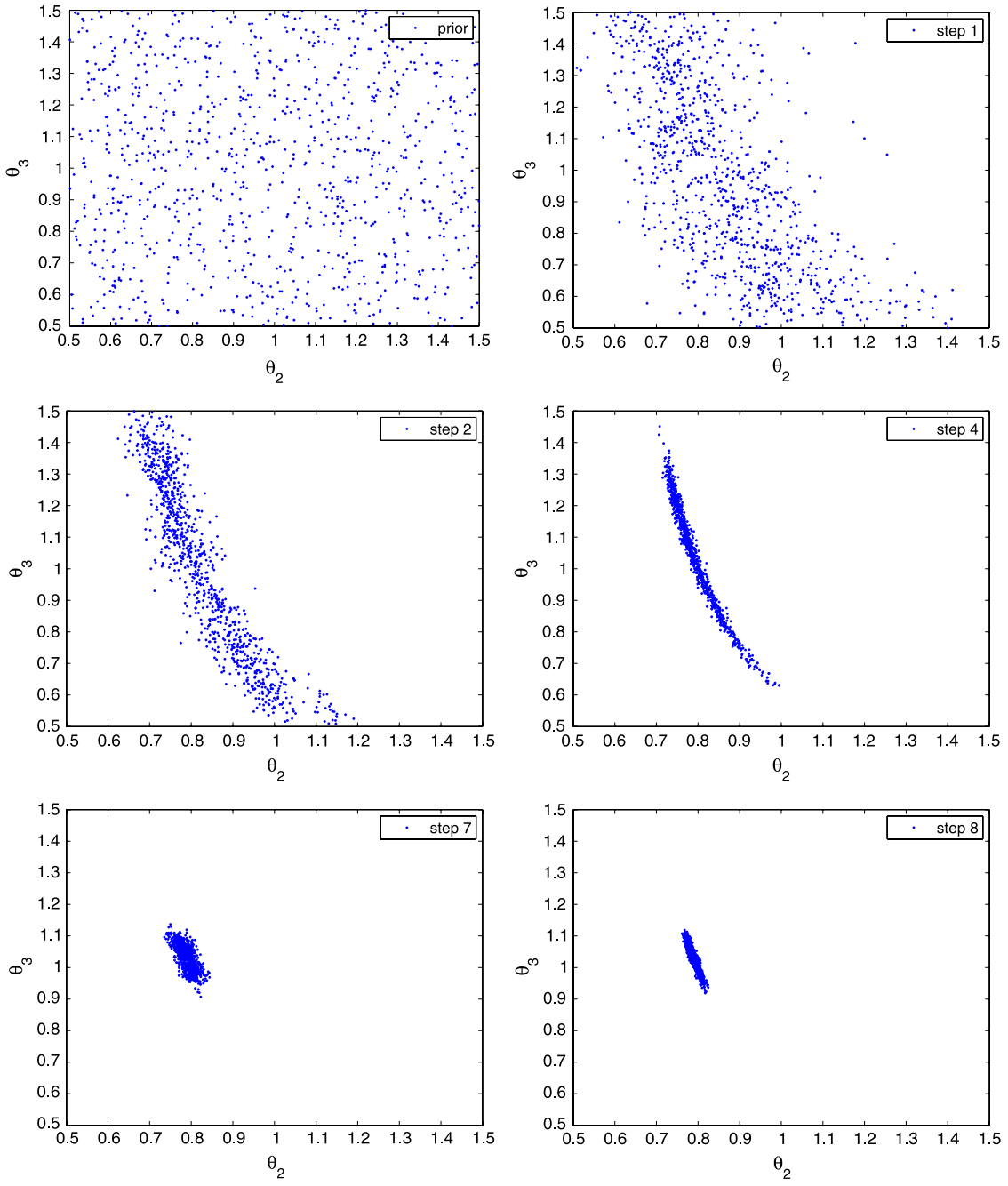

Fig. 8. Plots of the samples in the (θ_2–θ_3) space generated at different steps of the transitional Markov chain Monte Carlo method when updating model class $M^{(2)}$.

6.1.6. Computational cost

The number of finite element runs for each model class depends, among other things, on the number of transitional Markov chain Monte Carlo stages (steps) which in this case is equal to 8 for all three model classes. For comparison purposes, the computational effort for obtaining one dynamic response of the original unreduced finite element model is approximately 16 s. Multiplying this time by the total number of dynamic analyses required during the identification process the computational effort for each model class is expected to be of the order 4384 min (3 days). In contrast, for the reduced-order models the computational demands for running each of the three model classes are

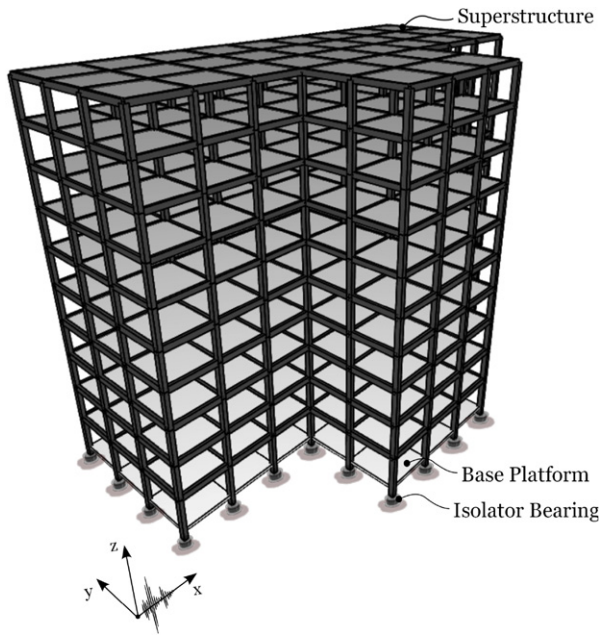

Fig. 9. Building model with base isolation system.

reduced to less than 4 h. Thus, a drastic reduction in computational efforts (more than one order of magnitude) is achieved without compromising the predictive capability of the proposed identification methodology. The previous computational efforts are based on the consideration of some parallelization features of the identification process. In particular eight transitional Markov Chain Monte Carlo samples are run simultaneously in the present implementation taking advantage of the available four-core multi-threaded computer unit.

6.2. Example 2: updating of linear model with localized nonlinearities

6.2.1. Structural model

A base-isolated structural system is considered in the second example. For this purpose the structural system described in the previous example is equipped with a total of 48 rubber bearings in its isolation system. The isometric view of the combined system (superstructure and base-isolation system) is shown in Fig. 9. The total mass of the platform is equal to 6.0×10^5 kg. The isolation devices (rubber bearings) consist of layers of rubber and steel, with the rubber being vulcanized to the steel plates. Fig. 10 shows a schematic representation of a rubber bearing, where D_e represents the external diameter of the isolator, D_i indicates the internal diameter, $H_r = t_r n_r$ is the total height of rubber in the device, where t_r is the layer thickness and n_r is the number of rubber layers. The nominal values of the isolator parameters are set equal to $\bar{D}_e = 0.85$ m, $\bar{H}_r = 0.14$ m, and $\bar{D}_i = 0.10$ m. These devices are able, in principle, to support the superstructure vertically, to provide the horizontal flexibility together with the restoring force, and to supply the required hysteretic damping. The force displacement characteristics of the isolator elements are modeled by a biaxial hysteretic behavior. An analytical model which is based on a series of experimental tests is used in the present application. A general description of the analytical model is provided in a subsequent section.

6.2.2. Response of the combined system

In general, base-isolated buildings are designed such that the superstructure remains elastic. Hence, the superstructure is modeled as a three dimensional linear elastic system while the base is assumed to be rigid in plane and it is modeled using three degrees of freedom. Let $\mathbf{u}_e(t)$ be the Nth dimensional vector of relative displacements of the superstructure with respect to the base, and $\mathbf{M}_e$, $\mathbf{C}_e$, $\mathbf{K}_e$ be the corresponding mass, damping and stiffness matrices, respectively. Also, let $\mathbf{u}_b(t)$ be the vector of base displacements with three components and $\mathbf{G}_e$ be the matrix of earthquake influence coefficients of dimension $N \times 3$, that is, the matrix that couples the excitation components of the

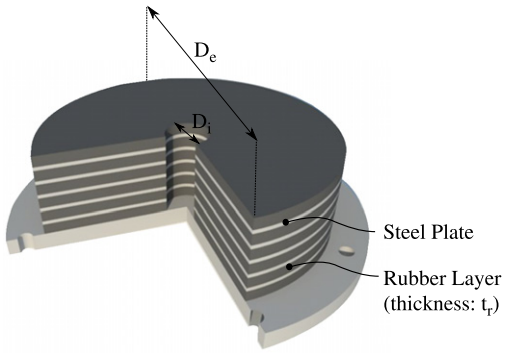

Fig. 10. Schematic representation of a rubber bearing.

vector $\ddot{\mathbf{u}}_g(t)$ to the degrees of freedom of the superstructure. The equation of motion of the superstructure is expressed in the form

$$\mathbf{M}_e\ddot{\mathbf{u}}_e(t) + \mathbf{C}_e\dot{\mathbf{u}}_e(t) + \mathbf{K}_e\mathbf{u}_e(t) = -\mathbf{M}_e\mathbf{G}_e[\ddot{\mathbf{u}}_b(t) + \ddot{\mathbf{u}}_g(t)] \tag{23}$$

where $\ddot{\mathbf{u}}_b(t)$ is the vector of base accelerations relative to the ground. On the other hand the equation of motion for the base platform is written as

$$(\mathbf{G}_e^T\mathbf{M}_e\mathbf{G}_e + \mathbf{M}_b)(\ddot{\mathbf{u}}_b(t) + \ddot{\mathbf{u}}_g(t)) + \mathbf{G}_e^T\mathbf{M}_e\ddot{\mathbf{u}}_e(t) + \mathbf{C}_b\dot{\mathbf{u}}_b(t) + \mathbf{K}_b\mathbf{u}_b(t) + \mathbf{f}_{rb}(t) = \mathbf{0} \tag{24}$$

where $\mathbf{M}_b$ is the mass matrix of the rigid base, $\mathbf{C}_b$ is the resultant damping matrix of viscous isolation components, $\mathbf{K}_b$ is the resultant stiffness matrix of linear elastic isolation components, and $\mathbf{f}_{rb}(t)$ is the vector containing the nonlinear forces activated on the isolators. If the dynamic response of the superstructure is represented by a linear combination of its mode shapes, that is, $\mathbf{u}_e(t) = \boldsymbol{\Upsilon}_e\boldsymbol{\eta}_e(t)$, where $\boldsymbol{\Upsilon}_e$ is the matrix of mode shapes of the superstructure and $\boldsymbol{\eta}_e(t)$ is the corresponding vector of modal response functions, the combined equation of motion of the base-isolated structural system can be written as

$$\begin{bmatrix} \mathbf{I} & \boldsymbol{\Upsilon}_e^T\mathbf{M}_e\mathbf{G}_e \\ \mathbf{G}_e{}^T\mathbf{M}_e\boldsymbol{\Upsilon}_e & \mathbf{M}_b + \mathbf{G}_e{}^T\mathbf{M}_e\mathbf{G}_e \end{bmatrix} \begin{Bmatrix} \ddot{\boldsymbol{\eta}}_e(t) \\ \ddot{\mathbf{u}}_b(t) \end{Bmatrix} + \begin{bmatrix} \mathbf{C}_{e\eta} & \mathbf{0} \\ \mathbf{0} & \mathbf{C}_b \end{bmatrix} \begin{Bmatrix} \dot{\boldsymbol{\eta}}_e(t) \\ \dot{\mathbf{u}}_b(t) \end{Bmatrix} + \begin{bmatrix} \mathbf{K}_{e\eta} & \mathbf{0} \\ \mathbf{0} & \mathbf{K}_b \end{bmatrix} \begin{Bmatrix} \boldsymbol{\eta}_e(t) \\ \mathbf{u}_b(t) \end{Bmatrix} = -\begin{bmatrix} \boldsymbol{\Upsilon}_e^T\mathbf{M}_e\mathbf{G}_e \\ \mathbf{M}_b + \mathbf{G}_e{}^T\mathbf{M}_e\mathbf{G}_e \end{bmatrix} \ddot{\mathbf{u}}_g(t) - \begin{Bmatrix} \mathbf{0} \\ \mathbf{f}_{rb}(t) \end{Bmatrix} \tag{25}$$

where the matrices $\mathbf{C}_{e\eta}$ and $\mathbf{K}_{e\eta}$ are given by

$$\mathbf{C}_{e\eta} = \begin{bmatrix} 2\xi_{e1}\omega_{e1} & & & \\ & \ddots & & \\ & & 2\xi_{ei}\omega_{ei} & \\ & & & \ddots \\ & & & & 2\xi_{em}\omega_{em} \end{bmatrix}, \qquad \mathbf{K}_{e\eta} = \begin{bmatrix} \omega_{e1}^2 & & & \\ & \ddots & & \\ & & \omega_{ei}^2 & \\ & & & \ddots \\ & & & & \omega_{em}^2 \end{bmatrix}$$

in which $\omega_{er}, r = 1, \ldots, m$, are the natural frequencies of the original system, $\xi_{er}, r = 1, \ldots, m$, are the corresponding damping ratios and $m \ll N$ is the number of modes considered. Note that the natural frequencies and mode shapes of the original model of the superstructure are obtained from the reduced-order system model (see Section 4.4). It is noted that the combined equation of motion (superstructure and base-isolation system) constitutes a nonlinear system of equations due to the nonlinearity of the isolation forces. The solution of the equation of motion (25) is obtained in an iterative manner by using any suitable step-by-step nonlinear integration scheme [37].

6.2.3. Base-isolation system

An analytical model that simulates measured restoring forces under bidirectional loadings is used in the present application to describe the nonlinear behavior of the isolators. The model is based on a series of experimental tests conducted for real-sized rubber bearings [41]. On the basis of the test results the analytical model assumes that the

restoring force on a rubber bearing is composed of a force directed to the origin of the isolator and another force approximately opposite to the direction of the movement of the isolator, that is, $\mathbf{f}_{\text{isolator}}(t) = -\hat{\mathbf{u}}(t) f_{\text{elastic}}(t) - \mathbf{d}(t) f_{\text{elastoplastic}}(t)$, where $\mathbf{f}_{\text{isolator}}(t)$ represents the forces activated on the isolator in the x and y direction, $\hat{\mathbf{u}}(t)$ is the unit directional vector of the isolator displacement vector $\mathbf{u}(t)$ in the x and y direction, $f_{\text{elastic}}(t)$ is the nonlinear elastic component of the force, $\mathbf{d}(t)$ is the direction of the movement of the isolator, and $f_{\text{elastoplastic}}(t)$ is the elastoplastic component of the force. The direction of the movement $\mathbf{d}(t)$ is defined in terms of the isolator displacement vector by means of the nonlinear differential equation [42,43]

$$\dot{\mathbf{d}}(t) = \frac{1}{\alpha}\|\dot{\mathbf{u}}(t)\| \left[\hat{\dot{\mathbf{u}}}(t) - \|\mathbf{d}(t)\|^n \hat{\mathbf{d}}(t)\right], \qquad \mathbf{u}(0) = \mathbf{0}, \qquad \mathbf{d}(0) = \mathbf{0} \tag{26}$$

where $\dot{\mathbf{u}}(t)$ is the velocity vector and $\hat{\dot{\mathbf{u}}}(t)$ and $\hat{\mathbf{d}}(t)$ are the unit directional vectors of $\dot{\mathbf{u}}(t)$ and $\mathbf{d}(t)$, respectively, and $\|\cdot\|$ indicates the Euclidean norm. Note that the isolator displacement vector $\mathbf{u}(t)$ can be obtained directly from the base displacement vector $\mathbf{u}_b(t)$. The parameters α and n are positive constants that relate to the yield displacement and smoothness of yielding, respectively. Based on a set of loading tests carried out for real-size bearings the parameters α and n are estimated as $0.2H_r$ and 0.7, respectively, where H_r is the total height of rubber, as indicated before. Next, the elastic component of the force $f_{\text{elastic}}(t)$ and the elastoplastic component $f_{\text{elastoplastic}}(t)$ are approximated as

$$f_{\text{elastic}}(t) = \begin{cases} 0.35A\gamma(t) & \text{if } 0 \le \gamma(t) \le 1.8 \\ 0.35A\gamma(t) + 0.2A(\gamma(t) - 1.8)^2 & \text{if } \gamma(t) \ge 1.8 \end{cases} \tag{27}$$

and

$$f_{\text{elastoplastic}}(t) = 0.125A + 0.015A\gamma(t) + 0.012A\gamma(t)^3 \tag{28}$$

where $A = \pi/4(D_e^2 - D_i^2)$ is the cross sectional area of the rubber and $\gamma(t) = \|\mathbf{u}(t)\|/H_r$ is the average shear-strain. It is noted that the linear component of the isolators forces represented by the matrix $\mathbf{K}_b\mathbf{u}_b(t)$ and the nonlinear forces activated on the isolators given by the vector $\mathbf{f}_{rb}(t)$ in Eq. (25) can be obtained directly from the characterization of the force on each isolator ($\mathbf{f}_{\text{isolator}}(t)$). Validation calculations have shown that the analytical model is able to accurately simulate the test results for both bidirectional and unidirectional loading [42]. For a detailed description and implementation of the analytical model that describe the nonlinear behavior of the isolators the reader is referred to [42,43].

6.2.4. Model updating problem

The structural system previously described is used for model updating using simulated response data. In particular the external diameter of the isolators D_e and the total height of rubber in the devices H_r are estimated. These parameters are parameterized as $D_e = \theta_1 \bar{D}_e$ and $H_r = \theta_2 \bar{H}_r$, where $\bar{D}_e = 0.85$ m and $\bar{H}_r = 0.14$ m are the corresponding nominal values. Note that these parameters control the value of the parameters α and A of the hysteretic model affecting the nonlinear behavior of the isolators. In addition, the stiffness of the columns of the first floor of the superstructure in the x direction is also estimated. This property is parameterized by the dimensionless parameter θ_3. In this application the superstructure is divided into two linear substructures as shown in Fig. 11.

Substructure 1 is composed by the column elements of the first floor while substructure 2 contains the rest of the superstructure components. In this context the base isolation system, that is, the isolation devices and the base platform, can be considered as a nonlinear substructure. As in the previous example, it is assumed that the base-isolated structural system is built and response data are available to update the isolator parameters and the stiffness of the columns of the first floor. The model updating is based on measurements of the ground acceleration at the support of the isolation system, the acceleration response in the x direction at the base platform and the acceleration response in the x direction at the first and the second floor. To this end the original unreduced finite element model of the combined system (superstructure and base-isolation system) is excited horizontally (in the x direction) with the Santa Lucia ground-motion record used in the previous example. The actual base-isolated system used to generate the simulated measured data is characterized as follows. The isolator parameters are set equal to $D_e = 0.78$ m, $H_r = 0.17$ m, and $D_i = 0.10$ m, and the stiffness of the superstructure columns of the first floor in the x direction is either kept fixed to its nominal value or is reduced by 20% with respect to its nominal stiffness value, depending on the model updating case considered (see later Section 6.2.5). It is noted that this model is more flexible than the nominal system since the

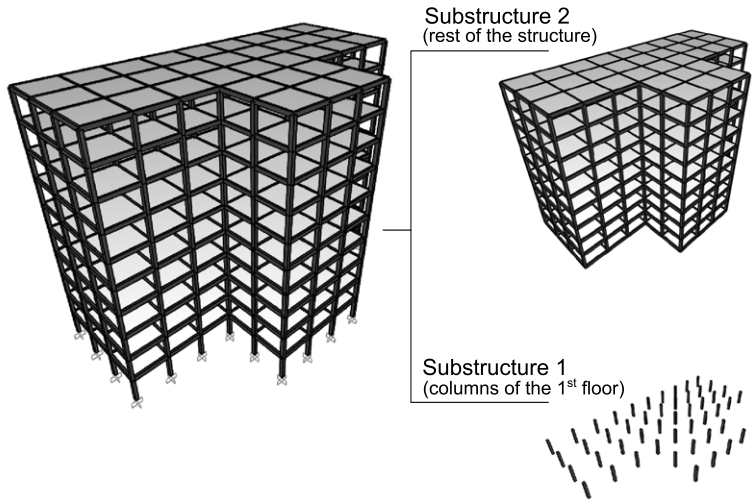

Fig. 11. Linear substructures of the superstructure finite element model used for model updating.

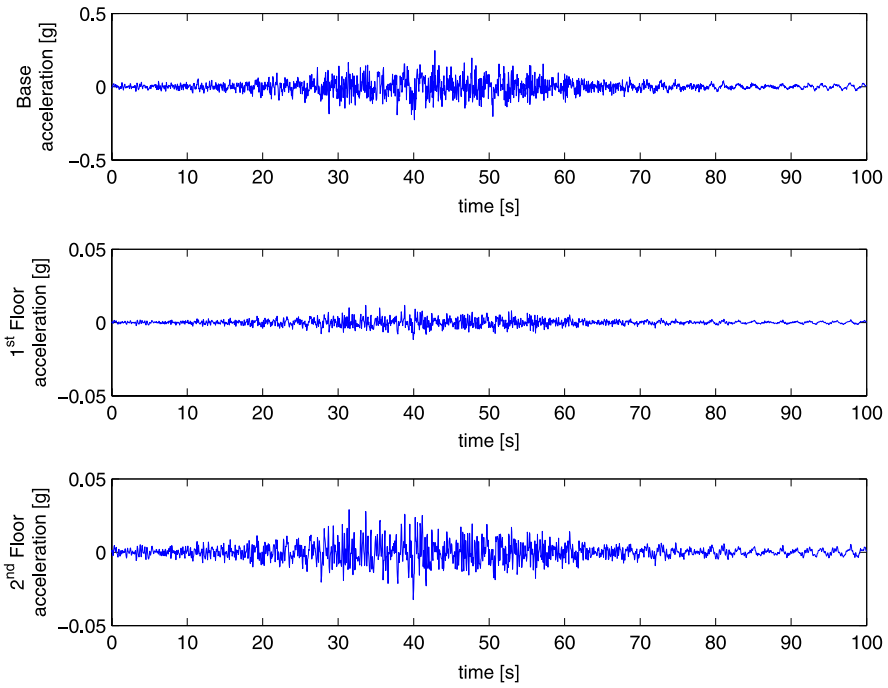

Fig. 12. Simulated acceleration time histories at the base platform, first floor, and second floor.

isolators have smaller external diameters and larger heights. Once the acceleration responses at the various locations are computed, a Gaussian discrete white noise is added with standard deviation equal to 10% of the root-mean square value of the corresponding acceleration time histories. One hundred seconds of data with sampling interval $\Delta t = 0.05$ s are used, given a total of $N_t = 2000$ data points. Simulated accelerations are plotted in Fig. 12 for the base platform and for the first and the second floor. For illustration purposes Fig. 13 shows a typical displacement—restoring force curve of one of the isolators. The nonlinear behavior of the isolators is clear from the figure.

The simulated response data shown in Fig. 12 provides the data for the model updating process. The actual implementation of this process is carried out by using a reduced-order system model which is defined as follows. For each linear substructure of the superstructure it is selected to retain all fixed-interface normal modes that have frequency less than a given cut-off frequency. As in the previous example, the cut-off frequency is set to be

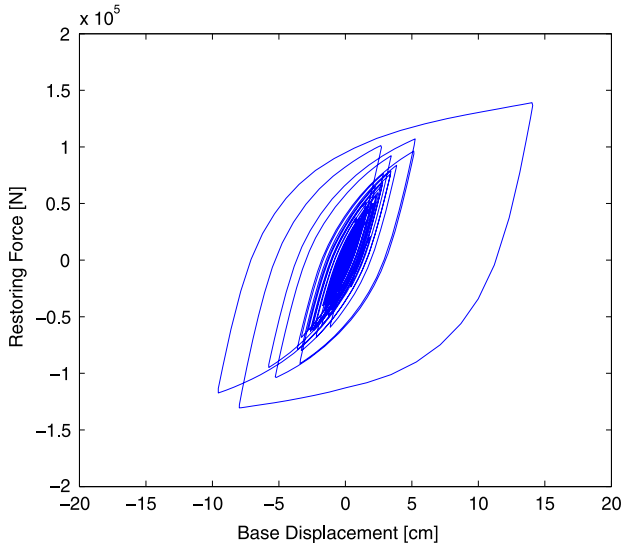

Fig. 13. Typical displacement—restoring force curve of one of the isolators.

proportional to the 12th modal frequency of the original unreduced superstructure finite element model. Validation calculations show that retaining 48 generalized coordinates for substructure 1 and 174 generalized coordinates for substructure 2 is adequate in the context of this application. In fact, with this number of generalized coordinates the fractional error (in percentage) between the modal frequencies using the complete finite element model and the modal frequencies computed using the reduced-order model fall below 0.1% for the lowest 12 modes. Then, a total of 222 generalized coordinates, corresponding to the fixed interface normal modes, out of 39,712 DOF of the original model are retained for the two linear substructures in this application. The number of interface degrees of freedom is equal to 288 in this case. The total number of degrees of freedom of the reduced model represents more than 98% reduction with respect to the unreduced model in this case.

6.2.5. Model updating results

Two cases are considered for the model updating problem. In the first case only the isolator parameters are identified with the provided data. To this end the dimensionless parameter θ_3 is set equal to 1, that is, there is no reduction in the stiffness of the first floor superstructure columns. Simulated measured data for this case are generated for $\theta_3 = 1$. In order to test the capabilities of the updating process in the framework of the combined system the identification of the isolator parameters as well as the stiffness properties of the superstructure are considered simultaneously in the second case. In the first case independent uniform prior distributions are assumed for the parameters θ_1 and θ_2 over the range [0.5, 1.4]. As previously pointed out these parameters affect the nonlinear behavior of the isolators. The number of samples at the different iteration steps of the transitional Markov chain Monte Carlo method is taken as 1000, that is $N_j = 1000,\ j = 1, \ldots, m$. The updating process converges in six stages (steps) in this case. The samples from the posterior probability density function are displayed in terms of the parameters θ_1 and θ_2 in Fig. 14.

The value of the nominal model parameters is also indicated in the figure. The large prior uncertainty about the parameters θ_1 and θ_2 (uniformly distributed over the range [0.5, 1.4]) is significantly reduced which is visible from the decreased range of the posterior samples. In fact the samples of the external diameter are distributed around the actual value of 0.78 m ($\theta_1 = 0.92$) while the samples of the total height of rubber are spread around the actual value of 0.17 m ($\theta_2 = 1.20$) as shown in the corresponding histograms of these parameters (Fig. 15). The results of Fig. 14 also suggest that the data for the updated isolation model result in uncertainties that are correlated along a certain direction. The correlation structure is consistent with the fact that the base isolation system becomes stiffer as the rubber diameter is increased. Contrarily, the isolation system becomes more flexible as the height of the rubber is increased [43]. Therefore, an increase in the rubber diameter is compensated by an increase in the height of the rubber during the updating process, and all points along that direction correspond to isolation system models that have similar base drift responses.

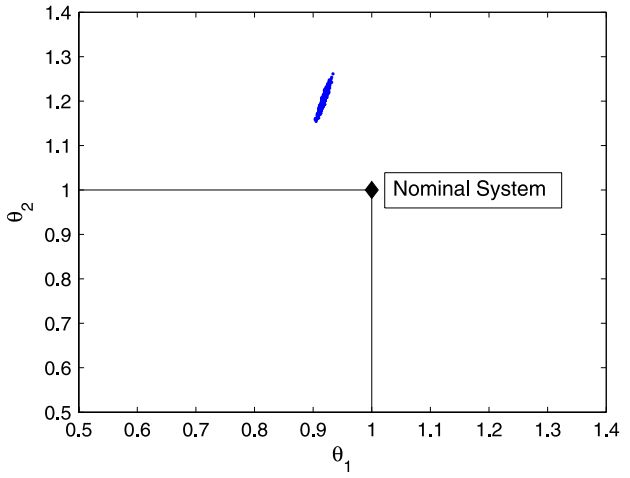

Fig. 14. Samples of the posterior probability density function in the (θ_1–θ_2) space generated at the last step of the transitional Markov chain Monte Carlo method.

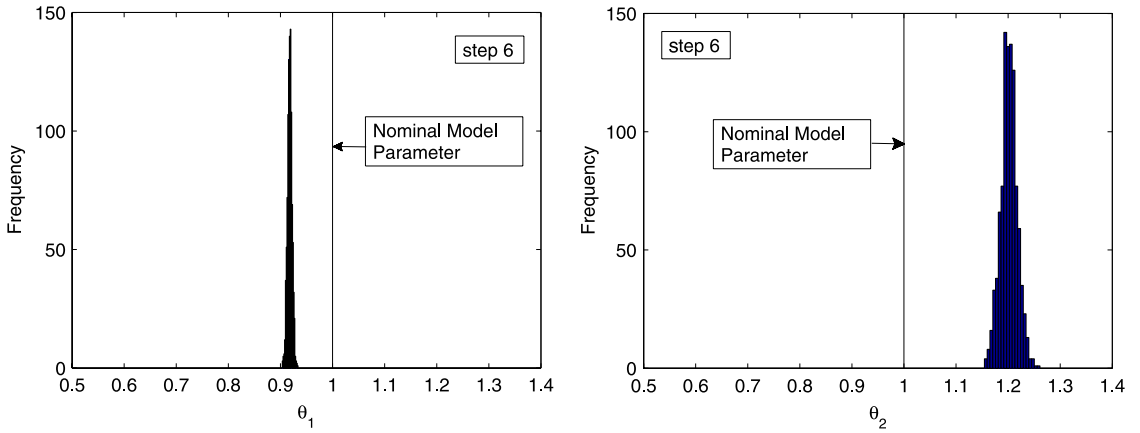

Fig. 15. Posterior histograms of model parameters θ_1 and θ_2. Mean estimates: $\bar{\theta}_1 = 0.92, \bar{\theta}_2 = 1.20$.

In the second case, the stiffness of the superstructure columns of the first floor in the x direction are identified together with the isolator parameters. Simulated data for this case are produced for $\theta_3 = 0.8$ (actual value). An independent uniform prior distribution defined over the interval [0.5, 1.5] is assumed for θ_3. Fig. 16 shows how the samples of the parameters θ_1, θ_2 and θ_3 converge during the updating process in terms of their histograms. After seven steps of the transitional Markov chain Monte Carlo method the parameters associated with the isolation system and the superstructure are distributed around their actual values $\theta_1 = 0.92, \theta_2 = 1.20$ and $\theta_3 = 0.80$. Actually, the mean estimate of these parameters are equal to $\bar{\theta}_1 = 0.92$, $\bar{\theta}_2 = 1.22$ and $\bar{\theta}_3 = 0.79$. From the different steps of the identification process it is clear that the posterior marginal distribution of the parameter related to the external diameter of the isolators is very peaked. Thus this parameter is identifiable to almost a unique value. This result is reasonable since this parameter has a significant effect on the global behavior of the combined system (isolation system and superstructure) [43]. On the other hand, the posterior marginal distributions of the parameters associated with the total height of rubber in the isolators and the stiffness of the first floor columns of the superstructure show some degree of dispersion around their mean estimates. This results is also observed in Fig. 17 where the projection of the samples in the (θ_2–θ_3) space are shown. From this figure the support of the unidentifiable domain is quite clear. Furthermore, there is no a clear interaction between these two parameters. This is consequent from a structural point of view since numerical validations have shown that the response of the base platform is not very sensitive to the total height of rubber in the isolators over the range considered here. Similarly, numerical simulations have demonstrated

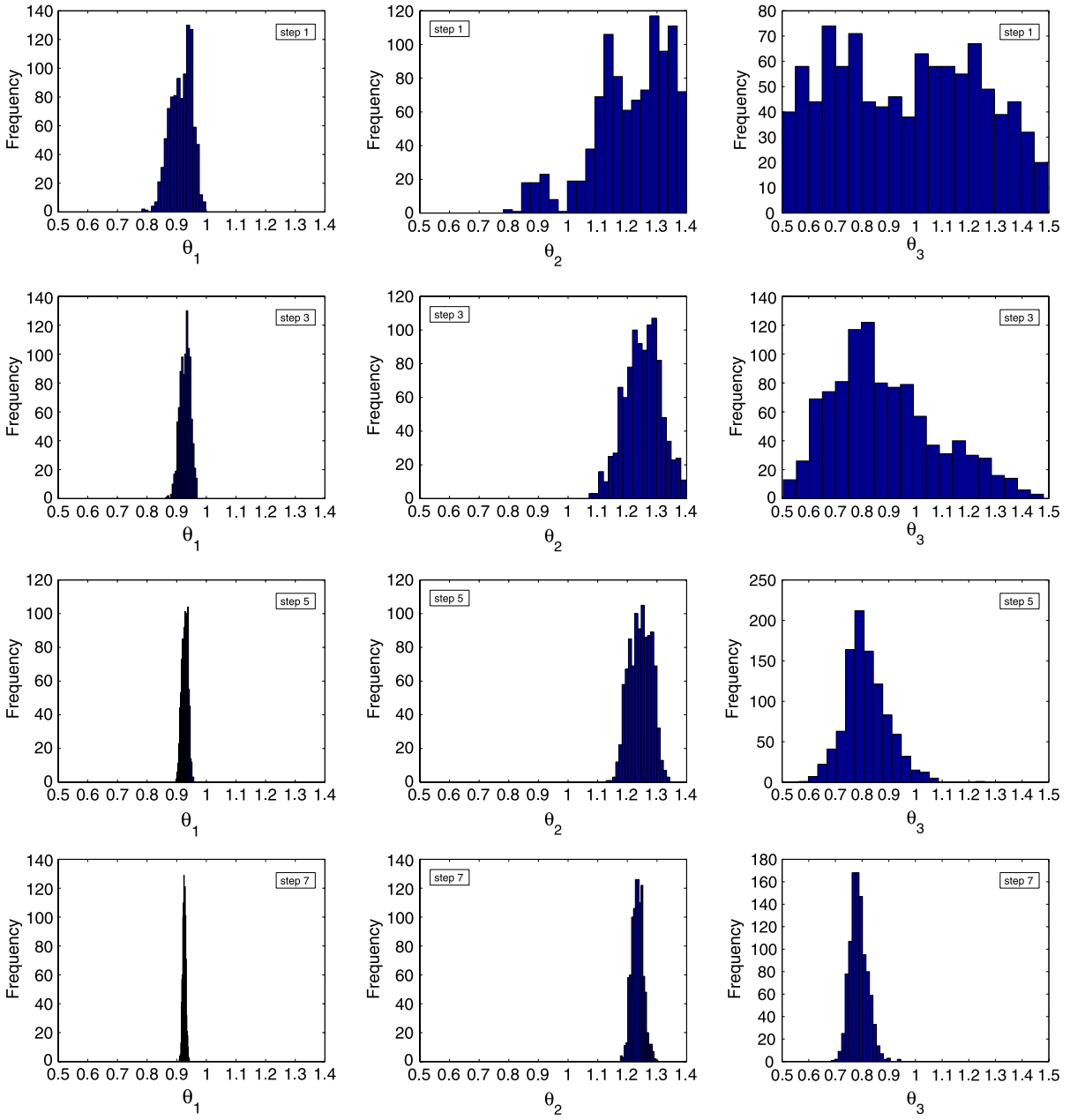

Fig. 16. Posterior histograms of model parameters θ_1, θ_2 and θ_3. Mean estimates at step 7: $\bar{\theta}_1 = 0.92$, $\bar{\theta}_2 = 1.22$, $\bar{\theta}_3 = 0.79$.

that the overall response of the combined system is relatively insensitive to the 20% stiffness reduction of the first floor superstructure columns. The previous results illustrate some important advantages of Bayesian updating procedures over traditional techniques that try to identify one best model when there is limited amount of data available. In this case the identification problem emerges as ill-conditioned without a unique solution for some parameters which can be tackled very efficiently by Bayesian model updating.

Finally, the computational demand for the updating process of the reduced-order combined system (isolation system and superstructure) is approximately 20 h. On the other hand the computational efforts using the unreduced finite element model is estimated to be almost six days. Thus, as in the previous example, the computational demands are drastically decreased by using the reduced-order model without compromising the predictive capabilities of the proposed updating procedure.

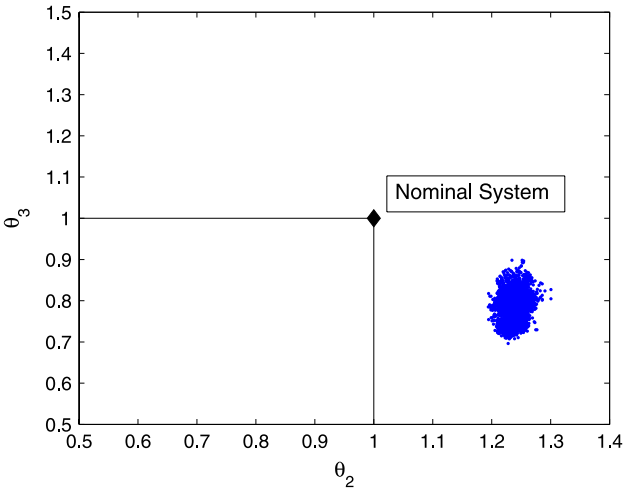

Fig. 17. Samples of the posterior probability density function in the (θ_2–θ_3) space generated at the last step of the transitional Markov chain Monte Carlo method.

7. Conclusions

A methodology that integrates a model reduction technique into a finite element model updating formulation using dynamic response data has been presented. In particular, a method based on fixed-interface normal modes and interface constraint modes of the linear substructures comprising the system with localized nonlinearities is considered in this work. In general, the method produces highly accurate models with relatively few substructure modes. The finite element model updating is carried out by using a simulation-based Bayesian model updating technique. Specifically, the transitional Markov chain Monte Carlo method is implemented in the present formulation. It is demonstrated that under certain substructuring schemes, often encountered in finite element model updating problems, the fixed-interface normal mode of each linear substructure and the characteristic interface modes are computed only once from a reference finite element model. In this manner the re-assembling of the reduced-order system matrices from linear substructures and interfaces modes is avoided during the updating process. Results show that the computational effort for updating the reduced-order model is decreased drastically by one or two orders of magnitude with respect to the unreduced model, that is, the full finite element model. Furthermore, the drastic reduction in computational efforts is achieved without compromising the predictive capability of the proposed identification methodology. Therefore it is concluded that the proposed approach is potentially an effective and useful tool for a certain class of Bayesian finite element model updating problems. Future research efforts aim at expanding the proposed formulation and increasing even further the computational savings. Specific issues to be considered include: the implementation of surrogate normal and constraint modes in order to consider more general cases as well as to reduce the number of reduced-order system re-analyses; and the implementation of the proposed scheme in a fully parallel environment to efficiently distribute the different computational tasks in available multi-core CPUs. Finally, the generalization of the proposed approach to different class of problems and different types of localized nonlinearities represents another future research effort.

Acknowledgments

The research reported here was supported in part by CONICYT under grant number 1110061 which is gratefully acknowledged by the authors. Also this research has been implemented under the “ARISTEIA” Action (grant number 53-UQ-dynamics) of the “Operational Programme Education and Lifelong Learning” and was co-funded by the European Social Fund (ESF) and Greek National Resources.

References

[1] Z. Zhao, A. Haldar, F.L. Breen, Fatigue-reliability updating through inspection of steel bridges, J. Struct. Eng. ASCE 120 (5) (1994) 1624–1641.
[2] R. Sindel, R. Rackwitz, Problems and solution strategies in reliability updating, J. Offshore Mech. Arct. Eng. 120 (2) (1998) 109–114.

[3] J.T.P. Yao, H.G. Natke, Damage detection and reliability evaluation of existing structures, Struct. Saf. 15 (1994) 3–16.
[4] G. Deodatis, H. Asada, S. Ito, Reliability of aircraft structures under nonperiodic inspection—a Bayesian approach, J. Eng. Fract. Mech. 53 (5) (1996) 789–805.
[5] C. Cremona, Reliability updating of welded joints damaged by fatigue, Int. J. Fatigue 18 (1996) 567–575.
[6] H. Shoji, M. Shinozuka, S. Sampath, A Bayesian evaluation of simulation models of multiple-site fatigue crack, Probab. Eng. Mech. 16 (2001) 355–361.
[7] P. Beaurepaire, M.A. Valdebenito, G.I. Schuëller, H.A. Jensen, Reliability-based optimization of maintenance scheduling of mechanical components under fatigue, Comput. Methods Appl. Mech. Engrg. 221–222 (2012) 24–40.
[8] H.O. Madsen, Model updating in reliability theory, in: Proc. ICASP 5, Vancuver, Canada, 1987.
[9] C. Papadimitriou, J.L. Beck, L. Katafygiotis, Updating robust reliability using structural test data, Probab. Eng. Mech. 16 (2001) 103–113.
[10] J.L. Beck, Bayesian system identification based on probability logic, Struct. Control Health Monit. 17 (7) (2010) 825–847.
[11] K.V. Yuen, Bayesian Methods for Structural Dynamics and Civil Engineering, John Wiley & Sons, 2010.
[12] N. Bleistein, R. Handelsman, Asymptotic Expansions for Integrals, Dover Publicactions, Inc., New York, NY, 1986.
[13] J. Beck, L. Katafygiotis, Updating models and their uncertainties. I: Bayesian statistical framework, J. Eng. Mech. 124 (4) (1998) 455–461.
[14] L. Katafygiotis, J. Beck, Updating models and their uncertainties. II: model identifiability, J. Eng. Mech. 124 (4) (1998) 463–467.
[15] S. Duane, A.D. Kennedy, B.J. Pendleton, D. Roweth, Hybrid Monte Carlo, Phys. Lett. B 195 (2) (1987) 216–222.
[16] J.L. Beck, S.K. Au, Bayesian updating of structural models and reliability using Markov chain Monte Carlo simulation, J. Eng. Mech. 128 (4) (2002) 380–391.
[17] J. Ching, Y.C. Chen, Transitional Markov chain Monte Carlo method for Bayesian updating, model class selection, and model averaging, J. Eng. Mech. 133 (2007) 816–832.
[18] S.H. Cheung, J.L. Beck, Bayesian model updating using hybrid Monte Carlo simulation with application to structural dynamic models with many uncertain parameters, J. Eng. Mech. 1135 (4) (2009) 243–255.
[19] K.V. Yuen, S.C. Kuok, Bayesian methods for updating dynamic models, Appl. Mech. Rev. 64 (1) (2011) 010802-1–010802-18.
[20] J.M. Nichols, E.Z. Moore, K.D. Murphy, Bayesian identification of a cracked plate using a population-based Markov chain Monte Carlo method, Comput. Struct. 89 (2011) 1323–1332.
[21] H.A. Jensen, C. Vergara, C. Papadimitriou, E. Millas, The use of updated robust reliability measures in stochastic dynamical systems, Comput. Methods Appl. Mech. Engrg. 267 (2013) 293–317.
[22] R.R Craig Jr., Structural Dynamics, An Introduction to Computer Methods, John Wiley & Sons, New York, 1981.
[23] C. Papadimitriou, D.Ch. Papadioti, Component mode synthesis techniques for finite element model updating, Comput. Struct. 126 (2013) 15–28.
[24] H. Jeffreys, Theory of Probability, third ed., Oxford University Press, USA, 1961.
[25] J.L. Beck, K.V. Yuen, Model selection using response measurements: Bayesian probabilistic approach, J. Eng. Mech. 130 (2) (2004) 192–203.
[26] E. Jaynes, Probability Theory: The Logic of Science, Cambridge University Press, 2003.
[27] E. Simoen, C. Papadimitriou, G. Lombaert, On prediction error correlation in Bayesian model updating, J. Sound Vib. 332 (18) (2013) 4136–4152.
[28] L.S. Katafygiotis, C. Papadimitriou, H.F. Lam, A probabilistic approach to structural model updating, J. Soil Dyn. Earthq. Eng. 17 (1998) 495–507.
[29] L.S. Katafygiotis, H.F. Lam, C. Papadimitriou, Treatment of unidentifiability in structural model updating, Adv. Struct. Eng. 3 (1) (2000) 19–39.
[30] B. Goller, J.L. Beck, G.I. Schuëller, Evidence-based identification of weighting factors in Bayesian model updating using modal data, in: ECCOMAS Thematic Conference on Computational Methods in Structural Dynamics and Earthquake Engineering, Rhodes, Greece, 2009.
[31] B. Goller, M. Broggi, A. Calvi, G.I. Schuëller, A stochastic model updating technique for complex aerospace structures, Finite Elem. Anal. Des. 47 (2011) 739–752.
[32] P. Angelikopoulos, C. Papadimitriou, P. Koumoutsakos, Bayesian uncertainty quantification and propagation in molecular dynamics simulations: a high performance computing framework, J. Chem. Phys. 137 (2012) 1441103-1–1441103-19.
[33] N. Metropolis, A. Resenbluth, M. Resenbluth, A. Teller, E. Teller, Equations of state calculations by fast computing machines, J. Chem. Phys. 21 (6) (1953) 1087–1092.
[34] W. Hastings, Monte Carlo sampling methods using Markov chains and their applications, Biometrika 57 (1) (1970) 97–109.
[35] R.R Craig Jr., M.C.C. Bampton, Coupling of substructures for dynamic analysis, AIAA J. 6 (5) (1965) 678–685.
[36] M.P. Castanier, Y.C. Tan, C. Pierre, Characteristic constraint modes for component mode synthesis, AIAA J. 39 (6) (2001) 1182–1187.
[37] J. Bathe, Finite Element Procedures, Prentice Hall, 2006.
[38] A.E. Sepulveda, H.L. Thomas, Improved transient response approximation for general damped systems, AIAA J. 34 (6) (1996) 1261–1269.
[39] H.A. Jensen, A.E. Sepulveda, Design sensitivity metric for structural dynamic response, AIAA J. 35 (9) (1998) 1286–1693.
[40] S.F. Gull, Bayesian inductive inference and maximun entropy, in: J. Skilling (Ed.), Maximum Entropy and Bayesian Methods, Kluwer, Dordrecht, Boston, MA, USA, 1989.
[41] S. Minewaki, M. Yamamoto, M. Higashino, H. Hamaguchi, H. Kyuke, T. Sone, H. Yoneda, Performance tests of full size isolators for super high-rise isolated buildings, J. Struct. Eng. AIJ 55(B) (2009) 469–477.
[42] M. Yamamoto, S. Minewaki, H. Yoneda, M. Higashimo, Nonlinear behavior of high-damping rubber bearings under horizontal bidirectional loading: full-scale tests and analytical modeling, Earthq. Eng. Struct. Dyn. 41 (13) (2012) 1845–1860.
[43] H.A. Jensen, D.S Kusanovic, M. Papadrakakis, Reliability-based characterization of base-isolated structural systems, in: European Congress on Computational Methods in Applied Sciences and Engineering, Vienna, Austria, 2012.